

SURFACE PLASMON RESONANCE INVESTIGATION OF SMALL MOLECULE
BINDING AND LARGE T-ANTIGEN INHIBITION IN THE
PRESENCE OF G-QUADRUPLEX
STRUCTURES

THESIS

Presented to the Graduate Council of
Texas State University-San Marcos in
Partial Fulfillment of the
Requirements

for the Degree

Master of SCIENCE

by

Matthew J. Decker, B.S.

San Marcos, Texas
May 2011

SURFACE PLASMON RESONANCE INVESTIGATION OF SMALL MOLECULE
BINDING AND LARGE T-ANTIGEN INHIBITION IN THE
PRESENCE OF G-QUADRUPLEX
STRUCTURES

Committee Members Approved:

Wendi M. David, Chair

Rachell E. Booth

L. Kevin Lewis

Approved:

J. Michael Willoughby

Dean of the Graduate College

COPYRIGHT

by

Matthew J. Decker

2011

FAIR USE AND AUTHOR'S PERMISSION STATEMENT

Fair Use

This work is protected by the Copyright Laws of the United States (Public Law 94-553, section 107). Consistent with fair use as defined in the Copyright Laws, brief quotations from this material are allowed with proper acknowledgment. Use of this material for financial gain without the author's express written permission is not allowed.

Duplication Permission

As the copyright holder of this work I, Matthew J. Decker, refuse permission to copy in excess of the "Fair Use" exemption without my written permission.

ACKNOWLEDGEMENTS

I would like to thank all of my committee members for their help during the pursuit of this project, especially Dr. Wendi David for her insight into the world of surface plasmon resonance. I would also like to thank my family for the support that they have provided me since childhood; I would not be where I am today if it were not for the traits that they have instilled in me over the years. I would like to thank Dr. Sean Kerwin and Dr. Dalip Kumar for providing necessary materials to conduct this research. Finally, I would like to thank Texas State University-San Marcos for providing me with the opportunity to pursue this project.

This manuscript was submitted on April 6th, 2011

TABLE OF CONTENTS

	Page
ACKNOWLEDGEMENTS	v
LIST OF TABLES	vii
LIST OF FIGURES	viii
CHAPTER	
I. INTRODUCTION	1
II. MATERIALS AND METHODS.....	17
III. RESULTS AND DISCUSSION.....	25
REFERENCES	50

LIST OF TABLES

Table	Page
1. DNA sequences.....	19
2. Inhibition of LTag with TMPyP4	28
3. Binding parameters of compound BM042.....	31
4. Binding parameters of compound BM043.....	33
5. Binding parameters of compound BM044.....	36
6. Binding parameters of compound 360.....	38
7. Binding parameter of compound BM042 in lithium.....	42
8. Summary of binding and inhibition data	49

LIST OF FIGURES

Figure	Page
1. SV40 LTag assembly at viral origin of replication (<i>ori</i>)	3
2. The four structural domains of SV40 LTag	5
3. Structural polymorphism of G-quadruplex DNA	7
4. Small molecule inhibitors of LTag	10
5. G-quadruplex interacting compounds	12
6. Surface plasmon resonance analysis	13
7. Determination of binding kinetics using SPR	15
8. Investigation of LTag inhibition with G-quadruplex interactive compounds	16
9. Determining half enzyme activity	27
10. Inhibition of LTag with TMPyP4	28
11. Compound BM042 concentration series	29
12. Evaluation of BM042 binding kinetics	31
13. Compound BM043 concentration series	32
14. Evaluation of BM043 binding kinetics	33
15. Compound BM044 concentration series	34
16. Evaluation of BM044 binding kinetics	35
17. Comparison of compounds (1 μ M)	36
18. Compound 360 concentration series	37

19. Evaluation of 360 binding kinetics	38
20. Spectroscopy for evaluating buffer effects on DNA topology	40
21. Compound BM042 lithium concentration series	40
22. Evaluation of BM042 binding kinetics	41
23. Lithium binding comparison of compounds	43
24. Evaluating SA chip condition	44
25. Determining decreased enzymatic activity	45
26. BM042 inhibition of LTag	46
27. BM043 inhibition of LTag	47
28. BM044 inhibition of LTag	47
29. 360 inhibition of LTag	48

CHAPTER I

INTRODUCTION

The replication of DNA is a vital process responsible for the transmission of genetic information to subsequent cell generations. In order to better elucidate this complex process, less complex organisms are often used as fundamental genetic and mechanistic models. Simian Virus 40 (SV40) has long been proven a useful model for studying eukaryotic replication for both its similarities in DNA replication and its decreased viral complexity. Consisting of multiple distinct elements, SV40 is able to utilize cellular components of the host while only requiring the production of a single virus encoded protein, large T antigen (LTag), for DNA replication and transformation (1, 2).

1. SV40 Large T Antigen

SV40, a simian virus, was accidentally introduced into the human population during the decade following 1955 by means of contaminated poliovirus vaccines. Since then, numerous publications have been produced aimed at the investigation of the viral method of transmission and its role in human carcinogenic activity (3). Assigned to the family *Papovaviridae*, from the fusion of the three representative viruses *Papilloma*, *Polyoma*, and *Vacuolating agent*, the SV40 virus contains circular double-stranded DNA

that codes for at least six viral proteins: LTag, small tumor antigen, an agnoprotein believed to be involved in assembly of viral particles and late messenger RNA (mRNA) processing, and three capsid proteins, VP1, VP2, and VP3 (4, 5). Cell infection begins with the binding of SV40 to a cell membrane receptor termed the major histocompatibility complex (MHC) where the viral capsid undergoes endocytosis and is transported to the nucleus (6). Upon entering the nucleus and uncoating viral DNA, transcription of the early region begins. SV40 mRNA is transcribed by host RNA polymerases and exported to the cytoplasm where it is translated by the host cell ribosome to produce, among other proteins, active LTag. This active protein is now capable of re-entering the nucleus where it performs two major functions: 1) It binds the viral origin of replication (*ori*), promoting the unwinding of the double helix and recruiting proteins essential to DNA synthesis including DNA polymerase α and replication protein A (RPA) (7, 8), and 2) It stimulates transcription from the late promoter and represses transcription of the early promoter, resulting in the gene products of the late region, VP1, VP2, and VP3, capsid proteins for virion assembly and viral exocytosis (9).

Utilizing ATP and Mg^{2+} , the multi-domain, multi-functional LTag assembles on the viral *ori* and stimulates DNA replication of the SV40 genome through bidirectional enzymatic unwinding, proceeding 3'-5' (10) (Figure 1). This viral origin consists of multiple distinct elements with the 64 bp core origin being sufficient for *in vitro* replication, although additional regulatory elements increase the efficiency of replication (11). Mutational analysis of this core origin DNA has identified three functional domains: a central palindrome (site II) that contains four 5'-GAGGC-3' sequence repeats, an

imperfect palindrome (EP) region on the SV40 early flank, and a 17 bp AT rich domain upstream of the central palindrome (12). The organization of the pentanucleotides within the central palindrome proves critical for optimal DNA unwinding with inverted pairs of repeats oriented toward a single base pair, central to the palindrome, denoted as nucleotide (nt) 1 on the SV40 map and a 1 bp spacer between each pentamer (2). Evidence demonstrates that LTag is capable of recognizing site II and binds specifically to at least two of the four pentanucleotides, and additional LTag monomers are recruited in the presence of ADP or ATP for double hexamer formation; however, pre-formed hexamers in solution may bind simultaneously at the *ori* (13, 14). This double hexamer is the functionally active form of LTag that results in untwisting of the AT tract, melting of the early palindrome, and then proceeding with bidirectional enzymatic unwinding.

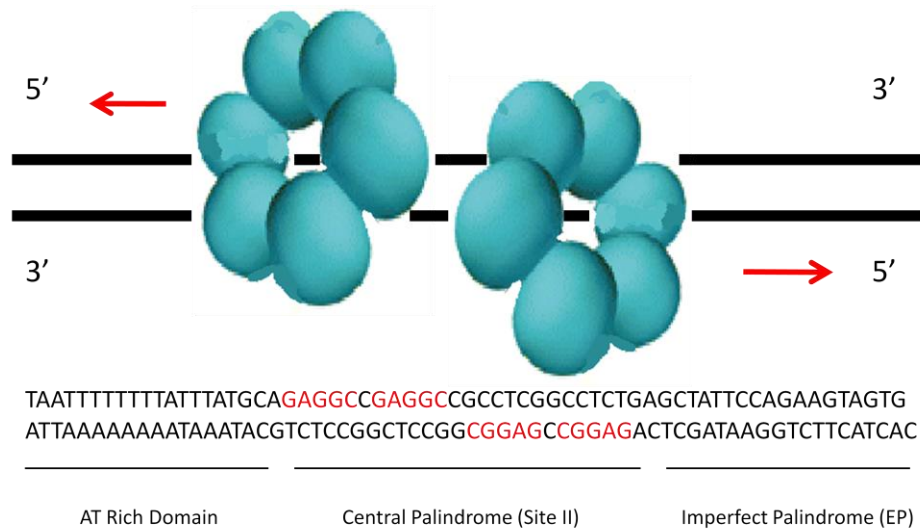


Figure 1. SV40 LTag assembly at viral origin of replication (*ori*). LTag assembles at Site II through recognition of the inverted pentanucleotides (red), eventually assembling a fully functional double hexamer for enzymatic bidirectional unwinding proceeding 3'-5'.

LTag is the SV40 encoded initiator and belongs to helicase superfamily III (SF3), a family of enzymes encoded mainly by small DNA viruses or large nucleocytoplasmic viruses (15). This protein consists of four structural domains beginning with an N-terminal J domain, a central origin binding domain (obd), a helicase domain, and finally, a C-terminal domain (Figure 2). The N-terminal region (amino acids 1-130) consists of approximately 80 amino acids with a 40 residue linker; and there is significant sequence similarity between the N-terminal domain and the conserved residues of type 3 DnaJ like proteins. Evidence shows that the N-terminal region of LTag is capable of binding known tumor suppressors such as retinoblastoma binding protein (pRB), requiring an LXCXE motif at amino acids 103 to 107 for stable association. pRB is a regulatory protein for the E2F complex (referring to any member of a family of transcription factors, 1-6), dependent upon phosphorylation by cyclin dependent kinase to regulate the synthesis of enzymes necessary for cell cycle progression. In addition, Hsc70, a protein known to inhibit apoptosis, has been shown to bind proximal to the pRB region, supporting the model that LTag is a link of Hsc70 to the RB-E2F complex (17). Furthermore, using molecular chaperone properties, the N-terminal region of LTag has been proven essential for viral activities including replication, transformation, transcriptional activation, and virion assembly (18). The LTag obd (residues 131-260) has the ability to vary between DNA binding and oligomerization to facilitate the requirements of recognition, melting, and unwinding during replication. This domain recognizes the *ori* sequence specific GAGGC pentamers allowing the enzyme to bind for replication. Residues within the LTag obd (amino acids 167, 213, 215, and 220) are capable of participating in

cooperative double hexamer assembly of the enzyme, leading to a fifteen fold increase in activity over the single hexamer form (19, 20). These hexameric rings contain a positively charged central channel large enough to accommodate duplex DNA with a diameter ranging from $\sim 7 \text{ \AA}$ (ATP bound) to $\sim 15 \text{ \AA}$ (apoenzyme form) (21). The helicase domain (amino acids 266-627) contains the enzymes helicase activity and x-ray crystallographic studies have revealed three structural sub-domains: a zinc domain, a highly conserved AAA+ helicase module (an acronym for ATPases Associated with diverse cellular Activities) for binding and hydrolyzing ATP, and a globular domain. It is believed that in addition to specific *ori* recognition by the obd, LTag assembly requires non-sequence specific contacts between these residues in the helicase domain and the flanking EP and AT rich regions (22). Finally, the C-terminal region (amino acids 628-708) is believed to aid in viral assembly and replication through interaction with host initiator protein topoisomerase I, to continuously relieve the superhelical tension created from DNA unwinding (23).

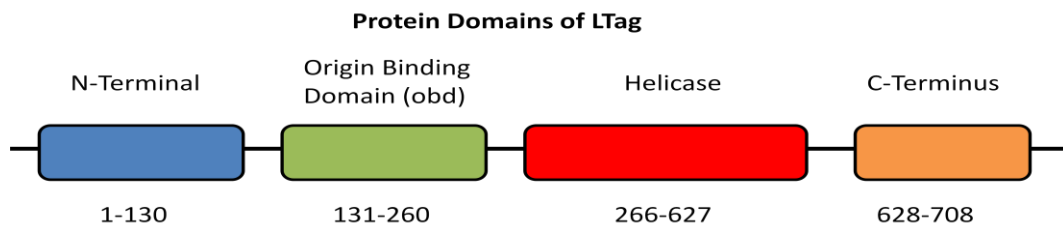


Figure 2. The four structural domains of SV40 LTag. The N-Terminal domain (blue, amino acid residues 1-130) is capable of interacting with various regulatory proteins. The obd (green, amino acid residues 131-260) facilitates binding and assembly of LTag. The helicase domain (red, amino acid residues 266-627) is responsible for enzymatic unwinding activity, association with ATP, and stabilization of the enzyme at the *ori*. The C-terminus domain (orange, amino acid residues 628-708) aids in viral assembly through interaction with topoisomerase I.

2. T-ag Possesses G-Quadruplex Helicase Activity

Knowing that LTag activity is essential for *in vivo* replication of the SV40 genome, it has become a focus of numerous scientific investigations into additional implications of its biological function. Much of this work has been accomplished through the use of synthetic duplex oligonucleotides that employ the necessary free 3' DNA substrate for efficient replication (24). However, in addition to duplex DNA unwinding, LTag has been proven to unwind synthetic quadruplex oligonucleotides (25). These non-canonical secondary structures consist of G-rich DNA sequences that use Hoogsteen base pairing to associate four G-bases into a cyclic tetrad structure that is capable of stacking to produce tetrad containing helical structures including unimolecular foldover structures, hairpin dimers, and parallel-stranded tetramers (26, 27) (Figure 3). Resulting from the interaction of one, two, or four strands of DNA, the formation of the quadruplex is stabilized by selective binding of a metal cation between successive tetrads (28); however, lithium has been shown to destabilize quadruplex formation and induce single-stranded DNA (29). The potential for quadruplex formation has been enumerated by several investigations with estimates of ~376,000 quadruplexes being able to exist simultaneously; however, actual quadruplex formation is likely much lower due to dynamic equilibrium of structural forms of DNA (30). While the significance of quadruplex helicase activity within the SV40 genome remains unclear, current evidence provides implications that quadruplex forming regions and helicases that are involved in maintaining these regions may play a role in genomic stability and association with proto-oncogenes.

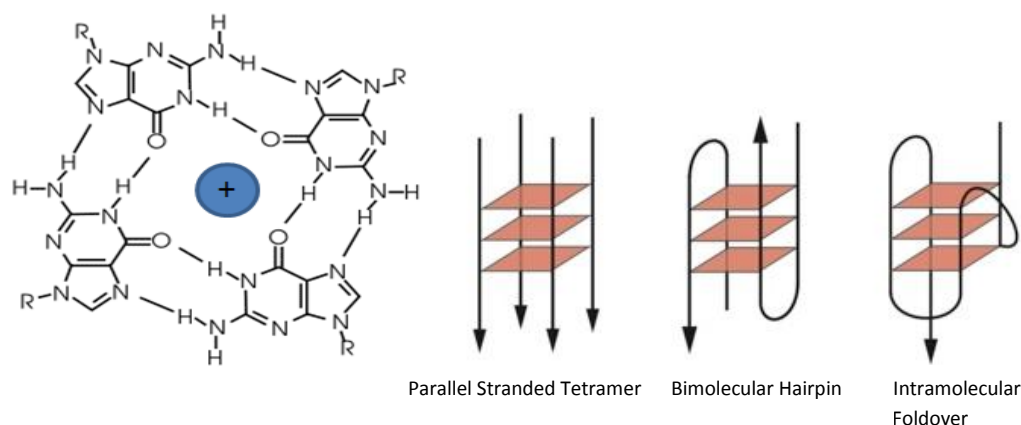


Figure 3. Structural polymorphism of G-quadruplex DNA. A centrally located cation between successive tetrads is necessary for G-quadruplex stability, with potassium providing the best coordination with the eight oxygens between two tetrads (far left, top down view of one tetrad). Three G-quadruplex structural variations are displayed beginning with a four stranded tetramer, a two stranded bimolecular hairpin, and a single stranded intramolecular foldover.

In addition to LTag, numerous other helicases have been shown to contain quadruplex unwinding capability. One such helicase sub-group includes members of the highly conserved RecQ family of helicases, with mutations within the genes of several of these family members having been linked to genomic instability, premature aging, and a dramatic predisposition to cancer. Werner syndrome is one example of a genetic disease encompassed by the loss of functionality of the RecQ helicase, WRN. Although the underlying molecular mechanism remains unclear, it has been reported that cells lacking WRN helicase functionality exhibit deletion of telomeres from single sister chromatids during lagging strand synthesis (31). These telomeric regions are known to possess vast G-rich sequences as evident from the telomeric repeat sequence $(T_2AG_3)_n$ as solved by NMR spectroscopy and X-ray crystallography (32, 33). G-quadruplexes formed in this region are potentially resolved by the WRN helicase to allow the replication fork to proceed through the telomeric region unimpeded, with a lack of WRN helicase activity

leading to stalling of lagging strand synthesis once the quadruplex structure is encountered. This event leads to loss of telomeric DNA and the induction of DNA damage machinery, forcing the cell into senescence much earlier than cells with functional helicase activity (34). While much remains to be learned, it is clear that the interaction of complexes with quadruplex structures plays a vital role in biological function.

Like their prevalence in telomeric regions, G-rich sequences can also be found in immunoglobulin class switch regions (S) and a region of the human c-MYC proto-oncogene, a commonly translocated transcription factor believed to regulate expression of ~15% of all genes (35). S regions are the sites of immunoglobulin class switch recombination and c-MYC has been shown to recombine with IgH switch regions to contribute to tumorigenesis by promoting deregulated expression of the c-MYC transcription factor (36). Translocations are induced rapidly upon expression of activation-induced deaminase (AID), a mutagenic factor that deaminates cytosine to uracil in DNA to initiate class switch recombination and has been shown to bind single-stranded regions of G-loops at c-MYC or switch regions (37). Therefore, this G-rich sequence composition is one feature of genomic structure capable of contributing to genomic instability and tumorigenesis, enhancing the significance of quadruplex structures and providing additional targets for chemotherapeutic agents.

Numerous potential anti-carcinogenic agents have been synthesized to inhibit known pathways associated with tumorigenesis. One such target is the enzyme telomerase, which is responsible for the elongation of human telomeric DNA through specialized reverse transcriptase function. This multi-domain enzyme carries the template for the 3' chromosomal addition of the repetitive T₂AG₃ motif in human telomeric

regions. Inactive in normal somatic cells, this enzyme is found in nearly 85% of all tumors and is essential for immortalization and tumorigenicity; however, the formation of quadruplex structures in telomeric DNA has been shown to inhibit the activity of the enzyme *in vitro* (38-40). Therefore, inhibition of this enzyme through stabilization of quadruplex structures has become a focus of study for anti-cancer therapy. Using biophysical methods such as the telomeric repeat amplification protocol (TRAP), which utilizes a PCR reaction to amplify products of telomerase, the IC_{50} of an inhibitory compound can be determined (41). G-quadruplex stabilizing telomerase inhibitors share similar structural features including large flat aromatic surface, cationic charges, and the ability for terminal stacking interactions. The necessity of aromatic preference for quadruplex DNA may be attributed to the increased surface area displayed by the G-quartet when compared to a typical base pair, with binding sites available at each end of the quadruplex for external stacking. However, rational design of these compounds becomes increasingly difficult due to G-quadruplex structural polymorphism from the numerous possible combinations of strands and loop length (42). Examples of these compounds include meso-tetra(*N*-methyl-4-pyridyl)porphine (TMPyP4), a cationic, planar molecule with proven affinity for quadruplex structures; and Distamycin A, a crescent-shaped pyrrole based compound (43) (Figure 4). Although the binding mechanism remains somewhat unclear, data supports both intercalation and end-capping mechanisms for binding TMPyP4 to quadruplex DNA, while Distamycin A utilizes its crescent shape for intercalation and groove binding interactions to G-quadruplex structures (44). Using the known interactions and mechanisms of nucleic acid ligands, the

synthesis and assessment of new compounds allows increased efforts toward the understanding of carcinogenic activity.

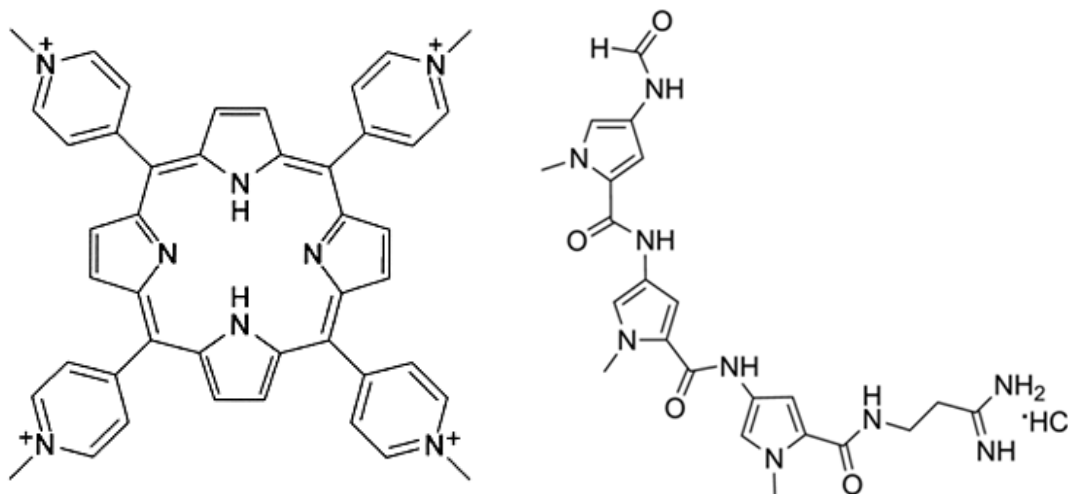


Figure 4. Small molecule inhibitors of LTag. TMPyP4 (left) is a porphyrin compound known to interact with G-quadruplex structures, stabilize these structures from thermal denaturation, and inhibit telomerase activity. Distamycin A (right) is a crescent shaped pyrrole structure that has been shown to intercalate between tetrads and the bases that flank quadruplex structures or to bind in the quadruplex groove.

Many G-quadruplex stabilizing telomerase inhibitors have also been shown to inhibit other G-quadruplex processing enzymes (45) and to interfere with genomic stability. The use of these compounds as therapeutic agents thus depends on their selectivity for particular enzyme inhibition, as well as selectivity for DNA topology.

3. Project Goal

Small molecules such as TMPyP4 have been proven to undergo interaction with G-quadruplex structures and contain inhibitory properties of the enzymatic activity of telomerase as evident by biochemical methods such as polyacrylamide gel

electrophoresis (PAGE), telomerase repeat amplification protocol, and/or fluorescence resonance energy transfer (FRET). These methods commonly involve the use of chemical markers such as bromoguanine substitutions with FRET analysis or radiolabels for PAGE techniques. These techniques have provided great insight into the analysis of enzymatic activity on intermolecular quadruplex structures, however, they lack the resolution necessary for observation of unimolecular structure unwinding in a label free manner and fail to provide thorough binding information of the compound to the substrate. Therefore, this project has used a technique called surface plasmon resonance (SPR) to investigate binding properties and LTag inhibition in a real-time, label-free environment. This technique provides the sensitivity necessary for detection of unimolecular quadruplex unwinding and allows the quantitation of binding information for determination of compound affinity for quadruplex structures.

Previous investigation of inhibition of LTag G-quadruplex helicase activity with TMPyP4 in our lab provided useful information for compound inhibition and established a repeatable inhibition assay for further use (46). This prompted the investigation of several novel compounds for their ability to selectively bind G-quadruplex structures and determination of binding kinetics that allows for elucidation of compound affinity for these structures (Figure 5). In addition, the selective G-quadruplex binding agent, 360, was characterized (47). These compounds were then investigated for their ability to inhibit the enzymatic activity of LTag in the presence of a G-quadruplex substrate, allowing for determination of structure/function relationships of each compound. By determining the inhibitory effects of each compound, a greater understanding of selective

binding to the G-quadruplex can be determined and allows for the possibility of improved chemotherapeutic agents in the future.

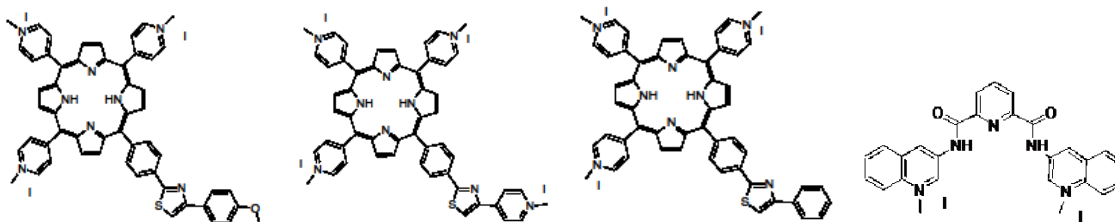


Figure 5. G-quadruplex interacting compounds. These compounds were synthesized with varying substituents and cationic charges to investigate binding affinity for G-quadruplex structures and inhibition of LTag enzymatic unwinding in the presence of an intramolecular quadruplex. From left to right, compounds BM042, BM043, BM044, and 360 all contain varying charge and structure that contribute to differing binding kinetics.

4. Research Strategy

Since the introduction of commercial surface plasmon resonance biosensors in 1990, additional devices using this optical technique have emerged to elucidate quantitative and qualitative characterizations of biological macromolecular interactions. This technique has proven attractive based on its ability to detect sub-nanomolar concentrations of reversible binding interactions, in real-time, without the necessity of a chromophoric group or radiolabel attachment to the macromolecule (48).

This technique employs a prism to generate polarized light with an increased wave vector capable of interacting with plasmons contained in a thin metal film, typically gold or silver. At a particular resonance angle, θ , a condition of total internal reflectance (TIR) is generated causing the excitation of nonradiative plasmons in the metal film. These plasmons become an oscillating longitudinal surface charge density wave that

travels along the metal surface as long as the angle of incidence remains capable of producing TIR. This resonance angle can be influenced by the addition of macromolecules to the sensor surface due to the refractive index profile of the sample above the sensor surface altering the local refractive index and producing a change in the resonance angle (49). This resonance angle change is measured in resonance units (RU), with 1 RU representing $\sim 1 \text{ pg protein mm}^{-2}$, and is plotted versus time to produce a binding progress curve called a sensorgram (50).

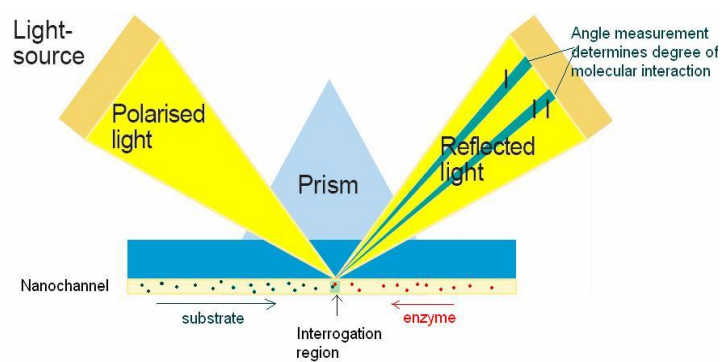


Figure 6. Surface plasmon resonance analysis. A diagram portraying surface plasmon resonance displays how substrate and enzyme can collaborate together upon injection into the nanochannel to determine compound interaction. As concentration changes at the interrogation region, the angle of reflected light must compensate to maintain TIR, thereby allowing the determination of compound binding/loss.

The strategy for typical SPR experimentation generally follows a relatively simple protocol. A substrate is first bound to the sensor surface, followed by an introduction of a mobile ligand to the buffer flow leading to an association with the substrate. Upon complex formation, disassociation of the complex begins as buffer lacking mobile ligand flows over the substrate causing time-dependent removal of the ligand and allowing the time-course of disassociation to be recorded. Finally, the sensor surface is regenerated

using a specific solution that provides ligand removal without excessive damage to the immobilized substrate. This procedure is then repeated using varying concentrations of ligand and can also be applied to enzymatic assays to observe potential inhibition.

The immobilization of substrate to the sensorchip surface can be accomplished by a variety of methods. Each sensorchip contains a 50 nm gold layer that is coated with a carboxymethylated dextran layer (100-200 nm) to provide improved accessibility of mobile ligand to the immobilized substrate and improved SPR signal through more efficient use of the evanescent field (51, 52). By derivatizing the dextran layer with varying functional groups, numerous potential substrates can be accommodated for immobilization. For our purposes, we utilized the strong attraction of biotin for streptavidin to immobilize biotinylated DNA onto a streptavidin coated sensorchip to form a tight, non-covalent bond with a K_D of 10^{-15} (M) (53).

Upon immobilization of an intramolecular G-quadruplex forming substrate on the sensor surface, investigation of novel compounds for G-quadruplex affinity was determined. All conditions necessary for G-quadruplex formation including proper buffer requirements and cation availability for stabilization were provided to ensure proper structure formation. Various concentrations of each compound were allowed to interact with the immobilized substrate for a determined period of time before regenerating the sensor surface to obtain valuable binding information for determining G-quadruplex affinity (Figure 7). Each sensorgram was subjected to evaluation using fitting algorithms provided by Biacore for determining kinetics based SPR analysis.

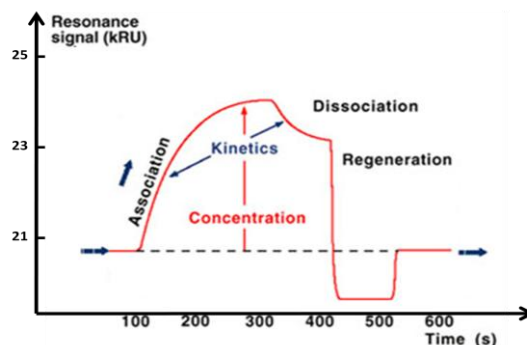


Figure 7. Determination of binding kinetics using SPR. As compound interacts with immobilized DNA, an association phase can be observed that produces an overall increase in RU due to the change in θ to maintain TIR. This is followed by dissociation of the compound, allowing determination of compound affinity for the substrate. The sensor surface is then regenerated and is ready for further use.

To better determine the inhibitory effects of G-quadruplex interactive compounds, the helicase activity of LTag was normalized prior to inhibitory investigations. An assay to determine half enzyme activity was performed by varying ATP concentration available for enzyme hydrolysis. Upon ascertaining a proper enzyme activity, various compounds were then introduced in the presence of an intramolecular G-quadruplex substrate to observe real-time effects of compound binding followed by LTag helicase unwinding and subsequent inhibition. Each immobilized substrate was hybridized with a partially complementary nucleotide sequence for determination of helicase unwinding (Figure 8). By observing the loss of substrate as evident by a change in RU, enzyme activity can be determined for each compound at a particular concentration. This real-time analysis provides a unique method for investigating inhibitory effects of G-quadruplex interactive compounds without the necessity of a marker or probe.

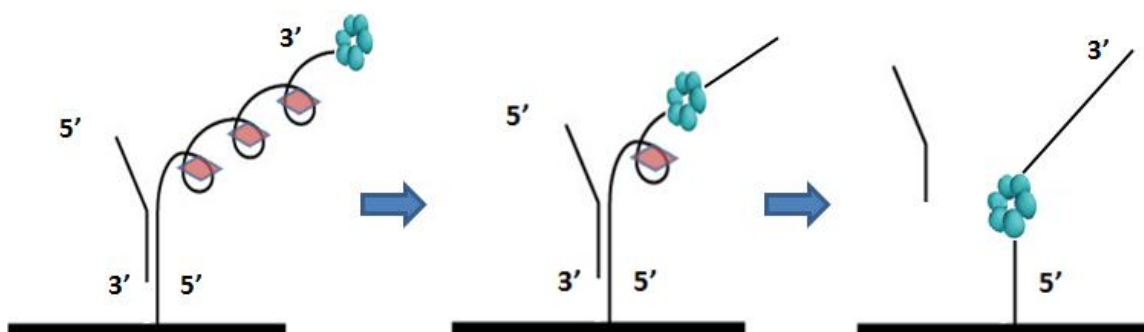


Figure 8. Investigation of LTag inhibition with G-quadruplex interactive compounds. A 5' biotinylated intramolecular G-quadruplex DNA substrate was immobilized to the SA sensorchip. The immobilized substrate was then hybridized with a partially complementary nucleotide sequence followed by injection of LTag. Enzymatic unwinding can be observed as loss of substrate upon helicase unwinding of the immobilized G-quadruplex substrate. However, if the compound under investigation is able to stabilize the quadruplex, diminished LTag can be observed through remaining hybridized oligonucleotide.

CHAPTER II

MATERIALS AND METHODS

1. Chemicals and Reagents

All reagents for buffer solutions were obtained from Sigma-Aldrich (St. Louis, MO) or GE Healthcare (Piscataway, NJ) unless otherwise noted. A working stock solution of 10x concentrated **HBS-EP Buffer** (0.1 M HEPES, 30 mM EDTA) was created for preparation of additional running buffers for experimental trials. Running buffers consisting of **HBS-EP-Mg²⁺ Buffer** (0.01 M HEPES, pH 7.4, 0.15 M KCl, 3 mM EDTA, 10 mM MgCl₂, and 0.005% v/v P20 surfactant), **HBS-EP-K⁺ Buffer** (0.01 M HEPES, pH 7.4, 0.15 M KCl, 3 mM EDTA, and 0.005% P20 surfactant) and **HBS-EP-LiCl₂** (0.01 M HEPES, pH 7.4, 0.01 M LiCl₂, 3 mM EDTA, and 0.005% P20 surfactant) were created prior to each experimental procedure. Potassium chloride was obtained from EM Science (Gibbstown, NJ) and magnesium chloride was obtained from ACROS Organics (Geel, Belgium). Any modification to these buffer stock solutions is noted in the individual method. All buffers were passed through 0.2 mm filters (Nalgene) and degassed under vacuum conditions for a minimum of ten minutes after buffer filtration.

Regeneration solutions for experimental trials were created for disassociation of analyte on the sensor surface using sodium hydroxide from EM Science, sodium chloride from Mallinckrodt (Phillipsburg, NJ), potassium chloride, lithium chloride and/or DMSO. Individual methods describe the concentration of regeneration solution used for each trial. All regeneration solutions were filtered and degassed under the same conditions as the running buffers mentioned previously.

DNA oligonucleotides were obtained from Integrated DNA Technologies (Coralville, IA) and HPLC purified. Each DNA oligonucleotide was stored at -20 °C and diluted with HBS-EP-K⁺ buffer to the indicated concentration prior to each use unless otherwise noted. These DNA oligonucleotides are tabulated in Table 1 and will hereafter be referred to according to the monikers in **bold** font.

SV40 LTag was obtained from CHIMERx (Milwaukee, WI), where it was isolated from cultured insect cells and stored in 10 mM Tris-HCl, pH 8.0, 100 mM NaCl, 1.0 mM EDTA, 1.0 mM dithiothreitol, and 50% (v/v) glycerol. LTag aliquots were created (aliquot 1: 1.3 µg/ µL, aliquot 2: 1.9 µg/ µL) and were used without further purification. All aliquots of the LTag enzyme were stored at -80 °C and diluted with HBS-EP-Mg²⁺ prior to each use. Adenosine 5'-triphosphate disodium salt was obtained from Sigma-Aldrich for enzyme hydrolysis and stored at -20 °C.

The small molecule TMPyP4 was used for enzyme inhibition studies and was obtained from Sigma-Aldrich. The small molecules BM042, BM043, BM044, and 360 were used for molecular binding assays and inhibition studies and were obtained as a gift from Dr. Dalip Kumar (BM series) at the Birla Institute of Technology and Science

(Rajasthan, India) and Dr. Sean Kerwin (360) at the University of Texas at Austin (Austin, TX). Each of these compounds were diluted in HPLC grade DMSO to their respective concentrations and stored under light sensitive conditions at 4 °C refrigeration until further dilution prior to experimentation.

Surface plasmon resonance experiments were performed using a Biacore® X instrument and streptavidin-derivatized (SA) sensor chips from GE Healthcare. Each sensor chip was stored at 4 °C until ready for use and allowed for sufficient capture of biotinylated nucleotides to observe real-time molecular interactions detected as a change in refractive index at the sensor chip surface. All experiments were performed at 25 °C unless otherwise noted.

Table 1. DNA sequences. Sequences containing a 5'-BioTEG linker were immobilized on SA sensor chips.

DNA	Sequence (Blue indicates complementarity to the preceding red sequence)
imG4	5'-BioTEG-TCGTGTATTGCTGCT(TTAGGG) ₄ TTTTTT-3'
imG4comp2	3'-CACATAACGACGATTT-5'
TAGcompG4	5'-TCGTGTATTGCTGCTTTTTTTT(TTAGGG) ₄ TTT-3'

2. Determination of Small Molecule Binding to DNA Substrates

2.1 Sensor Chip Preparation

SA sensor chips were pre-conditioned prior to immobilization of the desired nucleotide sequence by performing a series of three 20 μL injections of 1 M NaCl/50 mM NaOH in dual channel mode at 50 $\mu\text{L}/\text{min}$. HBS-EP- K^+ buffer was used as a running buffer and also served as the diluent for the DNA sequences to be immobilized. Upon dilution, biotinylated DNA was injected in 10-20 μL increments in single channel mode at 10 $\mu\text{L}/\text{min}$ until the desired immobilization level was achieved (\sim 100-150 RU). The sensorgram was then allowed to continue overnight to allow the DNA to equilibrate in buffer and immobilization level was calculated the following morning. During the course of all experiments, unless otherwise noted, one flowcell contained immobilized substrate of choice while the other was left blank for use as a reference cell. Regular maintenance including desorption with 0.5% (w/v) sodium dodecyl sulphate followed by 50 mM glycine pH 9.5 (GE Healthcare) and sanitization with dilute sodium hypochlorite was performed on the instrument between assays of different compounds.

2.2 Small molecule binding assay

Solid starting material of the small molecules BM042, BM043, BM044, and 360 were dissolved in 99.9% DMSO to obtain 10 mM concentrations of each. All compounds were kept under light sensitive conditions throughout the course of the experiment. A single flowcell of the SA sensor chip was then immobilized with imG4 DNA in HBS-EP- K^+ as described previously and allowed to equilibrate overnight. Equilibration under these conditions was previously shown in our lab to lead to intramolecular G-quadruplex

formation with imG4. Dilutions (500 nM – 5 μ M) of the chosen compound were then prepared immediately prior to each binding assay. Trials began by injecting each compound over a reference subtracted flowcell at 20 μ L/min for 180 seconds with a delayed wash of 180 seconds, beginning with the lowest concentration of each compound and increasing through the remainder of the trials. The sensorgram was allowed to proceed for a period of seven minutes after each injection had completely finished, including the wash, before regenerating the chip. After the seven minute period had elapsed, the flow rate was increased to 50 μ L/min and 1 M KCl/1 mM NaOH or 1 M KCl/50 mM NaOH were used to remove the compound. The efficiency of binding and the concentration of the compound were used to determine the strength of regeneration solution required. Each regeneration was complete when the initial RU value prior to addition of compound was achieved, making the SA chip accessible for the next trial.

Lithium buffer trials were also performed to assess the difference in selectivity of each compound for oligonucleotides with decreased quadruplex formation. Dilutions of each compound were generated in HBS-EP-LiCl₂ buffer and were kept under light sensitive conditions at 4 °C. The Biacore® X instrument was then heated to 40 °C over a period of one hour then allowed to cool back to 25 °C prior to binding analysis to ensure that potassium ion-stabilized quadruplexes were unfolded (quadruplex formation is greatly diminished in the presence of Li⁺ as opposed to potassium ion). Binding assays were performed as previously described with the exception that regeneration was accomplished using 1 M LiCl₂/50 mM NaOH.

Reference subtracted sensorgrams of varying concentrations of individual compounds were analyzed by BiaEvaluation software from Biacore for analysis of

binding kinetics including rates of association (k_a), dissociation (k_d), affinity for the substrate (K_A), and tightness of fit (K_D), then fitted with a Chi^2 value for determination of fit.

Oligonucleotide samples for CD spectroscopy were prepared at a 4 μM concentration using TAGcompG4 DNA in both HBS-EP- K^+ and HBS-EP- LiCl_2 buffers at pH 7.4 to observe spectrum differences with varying cations. CD spectra were obtained using a Jasco J-710 spectropolarimeter conducted at 25 $^\circ\text{C}$ in 1 mm pathlength cuvettes over a 225-345 nm wavelength range. Lithium buffer samples were heated to 90 $^\circ\text{C}$ in a hot water bath and allowed to cool to room temperature prior to analysis.

3. Determination of Quadruplex Helicase Activity and Inhibition

3.1 Preparation of G-quadruplex substrates

The sensor chip was first pre-conditioned as previously described and diluted imG4 DNA was immobilized onto one flow cell of the SA chip through the biotin/SA linkage until the desired response was reached (~400 RU). Upon equilibration, a solution of partially complimentary DNA sequence, imG4comp2, was then diluted in HBS-EP- K^+ buffer and injected over both flow cells until complete hybridization was observed. The response indicating maximum hybridization was calculated from equation (1):

$$R_{\text{max}} = \text{RU}_{\text{im}} * (\text{MW}_A/\text{MW}_L) * S \quad (\text{Eq. 1})$$

In this equation, R_{max} represents the response indicating 100% hybridization of imG4comp2 to the immobilized substrate, RU_{im} is the response observed upon

immobilization of the biotinylated single-stranded DNA (imG4), MW_A represents the molecular weight of the complementary DNA oligomer (imG4comp2), and MW_L is the molecular weight of the immobilized single-stranded DNA (imG4). Due to a 1:1 binding interaction between each DNA oligomer, multiplication of the R_{max} value by the binding stoichiometry factor (S) is not necessary.

3.2 Determining diminished LTag helicase activity

An assay to determine reduced enzyme activity was performed to better analyze the effects of small molecule inhibitors on LTag. Immobilization of imG4 DNA was performed as described previously and hybridization of the partially complementary oligomer, imG4comp2, was performed to achieve full hybridization. Varying concentrations of LTag were then injected to determine an optimal enzyme concentration that allowed reproducible enzyme activity. Each assay began with stabilization of the sensorgram in HBS-EP- K^+ buffer following hybridization. The buffer was then changed to HBS-EP- Mg^{2+} followed by multiple washes to introduce new buffer into the flowcell. Upon stabilization, ATP/LTag were mixed in a 1:1 fashion, in which LTag hexamer concentration was varied while ATP concentration remained constant (15 mM), and were injected at 20 μ L/min for 40 seconds. Upon completion of the injection, the enzyme activity was calculated using equation (2) and the chip was rehybridized to begin the next trial.

$$RU_{Unwound}/RU_{Hybridized} * 100 = \% \text{ Enzyme Activity} \quad (\text{Eq. 2})$$

3.3 Inhibition of LTag G-quadruplex helicase activity

Inhibition of LTag G-quadruplex helicase activity was demonstrated using varying concentrations of small molecule G-quadruplex interactive compounds. These compounds were prepared and stored under light sensitive conditions to prevent possible induction of nucleic acid photocleavage properties. Specific dilutions were created prior to beginning each assay and a sensorgram was initiated in HBS-EP-K⁺ buffer followed hybridization with a partially complementary oligonucleotide. Upon stabilization, the buffer was changed to HBS-EP-Mg²⁺ buffer prior to assessing enzyme activity and multiple washes were done to introduce new buffer into the flowcell. Stabilization must then occur post-buffer change (20-30 minutes) and ATP (30 mM) and LTag dilutions (2.0-2.93 nM) were created at this time. Next, 40 μ L of the desired concentration of inhibitory compound was injected using manual inject mode at 20 μ L/min for 120 seconds. This injection was paused upon completion of introducing the inhibitory compound, followed by an immediate injection of 1:1 mixture of ATP (15 mM)/LTag (1.0-1.46 nM) was injected and the manual injection was resumed. The injection was stopped at the completion of the LTag injection and the percent quadruplex unwound was calculated using equation (3). The flow rate was then increased to 50 μ L/min and the sensor chip was regenerated using two 30 μ L injections of 1 M KCl/50 mM NaOH. The SA chip was then ready to begin the next inhibition trial.

$$RU_{\text{Unwound}} / (RU_{\text{Hybridized}} * \% \text{ Enzyme Activity}) * 100 = \% \text{ Normalized Enzyme Activity}$$

(Eq.3)

CHAPTER III

RESULTS AND DISCUSSION

The major goal of this research was to determine the binding kinetics and quadruplex interactions of novel compounds for the continuation of advancement in our knowledge of G-quadruplex interactive small molecules. Each small molecule contained a varying structural element such as cationic charge or substituent group attachment to provide additional information regarding quadruplex selectivity based on molecular orientation. These molecules were evaluated for their intrinsic binding parameters such as association rates, dissociation rates, and overall affinity for the G-quadruplex structure. Observation of these parameters allowed determination of the effectiveness of each compound at interacting with the substrate and provided empirical evidence for the creation of new molecules.

The molecule TMPyP4 is an inhibitor of the enzyme telomerase, presenting its potential for an antitumor therapy drug. Using a radiolabeled substrate and HeLa cell extracts, Wheelhouse et al. were able to determine the IC_{50} of TMPyP4 against human telomerase to be 6.5 μ M (54). TMPyP4 has also been shown to inhibit the helicase activity of LTag (55). Here, we present the inhibition of LTag enzymatic activity

with TMPyP4 and several novel analogs using a real-time optical technique, surface plasmon resonance. The binding and inhibition by the G-quadruplex selective compound, 360, was also compared.

1. LTag G-quadruplex Helicase Activity Determined by Surface Plasmon Resonance

An assay to determine decreased enzyme activity was performed using a variable ATP concentration to determine a ~50% LTag enzyme activity in the presence of an intramolecular G-quadruplex. This assay was accomplished by a former graduate student, Fatemah Sanjar, and was vital for continuation of inhibition trials. By reducing the LTag enzymatic activity, we were better able to observe the inhibitory effects of each compound assayed, as full enzyme activity would often lead to complete unwinding of the G-quadruplex and subsequent release of the complementary nucleotide as described in chapter I. Ranges of ATP concentration (5-40 mM) were tested with 1.46 nM LTag, with a 15 mM concentration of ATP providing 50% enzyme activity (Figure 9). An SA sensorchip was used with ~415 RU of immobilized imG4 DNA, followed by full hybridization with the complementary imG4comp2 DNA (123 RU). For all experiments using this approach, the partially complementary oligonucleotide contains a free 5' end to minimize the potential for helicase loading, ensuring that LTag is forming a complex on the free 3' end of the immobilized DNA substrate. Using Equation (2), we were able to calculate the amount of enzyme activity based upon the amount of DNA removed.

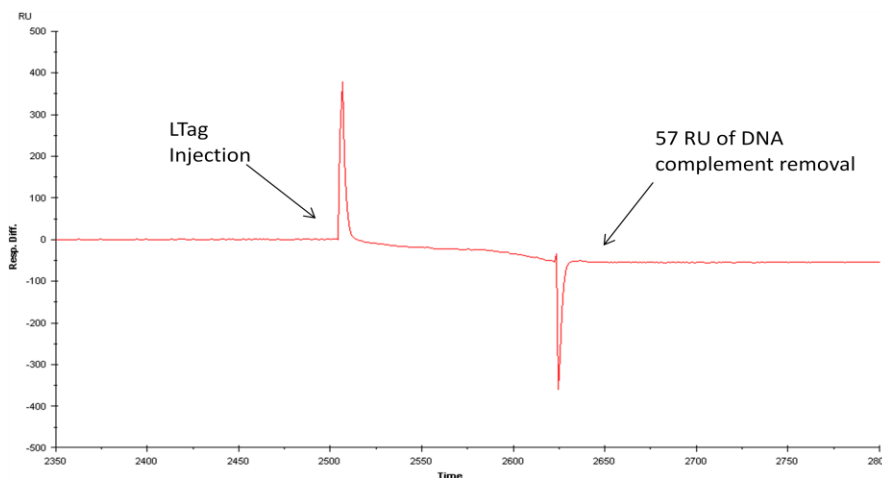


Figure 9. Determining half enzyme activity. This assay used varying concentrations of ATP to determine half enzyme activity in the presence of G-quadruplex structures. This figure contains ~123 RU of hybridized imG4comp2 DNA and following LTag injection, 57 RU are removed providing a 46% activity. Each trial is reference subtracted and performed on an SA chip in HBS-EP-Mg²⁺ buffer.

2. Inhibition of LTag G-quadruplex Helicase Activity by TMPyP4

The small molecule TMPyP4 was assayed for its ability to inhibit the enzymatic G-quadruplex helicase activity of LTag. TMPyP4 binding assays were completed by former graduate students and it is well known that the molecule has affinity for G-quadruplex structures and inhibits quadruplex helicase activity (46). By immobilizing imG4 DNA to the SA sensorchip as described in chapter I, and introducing a partially complementary oligonucleotide that would *only be removed* by LTag *if the intramolecular quadruplex structure was unwound*, we constructed a probe for determination of LTag enzymatic activity. Each trial was performed in HBS-EP-Mg²⁺ buffer to provide LTag with all necessary components for helicase functionality. The sensorchip was immobilized with ~700 RU of imG4 followed by full hybridization of imG4comp2 (206 RU). Upon injection, release of the DNA complement was observed and calculation of enzymatic activity was performed using equation (3) (Table 2).

TMPyP4 at 1 μM and 4 μM was used for the inhibition assays, with 4 μM providing nearly a 3 fold decrease in enzyme activity (Figure 10). These results prove the interaction of TMPyP4 with the intramolecular G-quadruplex DNA substrate and correlate with previous research indicating TMPyP4 inhibitory effects (54).

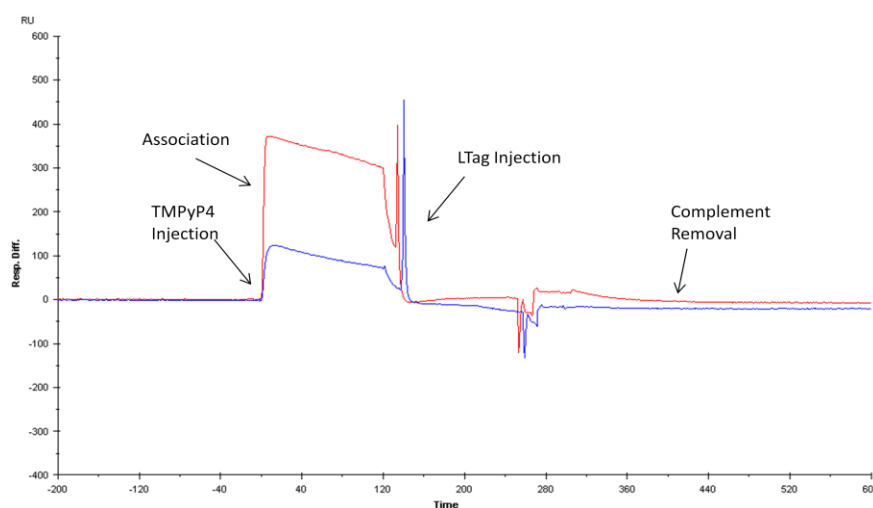


Figure 10. Inhibition of LTag with TMPyP4. Injections of 1 μM (blue trace) and 4 μM (red trace) TMPyP4 were injected at 20 $\mu\text{L}/\text{min}$ for 120 seconds immediately followed by 1.46 nM LTag for observation of enzyme inhibition. Each reference subtracted sensorgram contained ~ 700 RU of immobilized imG4 DNA, fully hybridized with imG4comp2 DNA. At 50% activity, full complement removal would reduce the response by ~ 103 RU. A removal of 8 RU (4 μM) and 24 RU (1 μM) displays the inhibition of each compound.

Table 2. Inhibition of LTag with TMPyP4. Each concentration, 1 μM and 4 μM , were assessed for their ability to inhibit LTag activity in the presence of an intramolecular quadruplex substrate.

Concentration	Enzyme Activity
1 μM	23%
4 μM	9%

n=2

3. Other G-quadruplex Interactive Compounds

3a. Determination of compound binding to an intramolecular G-quadruplex substrate.

The novel compounds BM042, BM043, BM044, and 360 were assayed for their ability to bind an intramolecular G-quadruplex structure. A concentration series of each compound was injected in HBS-EP-K⁺ buffer in the presence of immobilized imG4 DNA. The amount of immobilized substrate was kept ~150 RU to minimize the effects of mass transfer and provide the best possible binding information. No hybridized complement was necessary for each of these assays, as binding to the intramolecular quadruplex alone was of interest. The trials began with the introduction of BM042 in a concentration series (Figure 11). Concentrations of 750 nM – 5 μ M were prepared and kept under light sensitive conditions. Each compound was allowed to interact with the DNA for a determined period of time as described in chapter II.

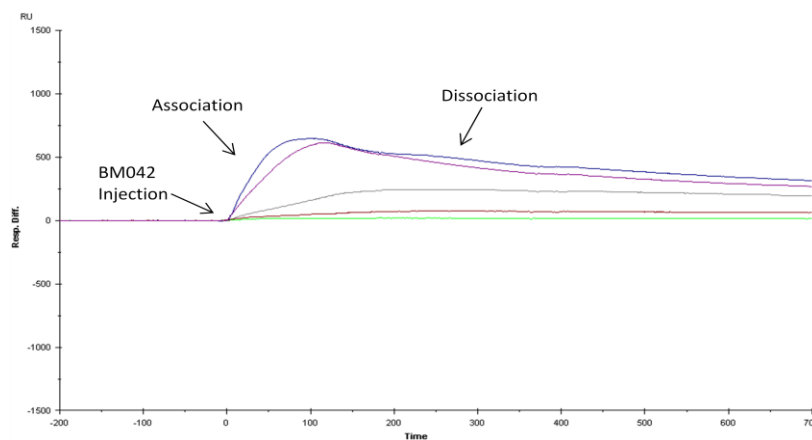


Figure 11. Compound BM042 concentration series. The compound BM042 was injected at 20 μ L/min in HBS-EP-K⁺ buffer with varying concentrations consisting of 5 μ M (blue trace), 2 μ M (magenta trace), 1 μ M (grey trace), 900 nM (maroon trace), and 750 nM (green trace). Each reference subtracted sensorgram represents binding of BM042 at the indicated concentration to ~150 RU of imG4 DNA to observe binding kinetics.

Upon completion of the assay, each reference subtracted sensorgram was then plotted in BiaEval to obtain binding parameters for determination of G-quadruplex affinity (Figure 12). The association, dissociation, and binding affinity for the G-quadruplex were determined for the concentration series. Compound BM042 appeared to have a relatively slow association, $k_a = 305$ (1/Ms), with the G-quadruplex, but was greatly enhanced as higher concentrations of the molecule were used indicating the potential for cooperative binding or aggregation of BM042 on the DNA substrate. This molecule contains three cationic charges at 3 of the porphyrin 'arms' and has a methoxy-substituted phenyl group appended to the 4th 'arm'. It is possible that the presence of this group may initially restrict access of the compound to the quadruplex structure, but it likely interacts with a groove of the quadruplex structure after initial binding is established. Although this compound exhibited a slow rate of association, the dissociation of the compound is the slowest of all compounds assayed, $k_d = 1.66e-5$ (1/s), showing that upon interaction with the immobilized DNA, the compound forms a tight interaction with a $K_D = 5.45e-8$ (M).

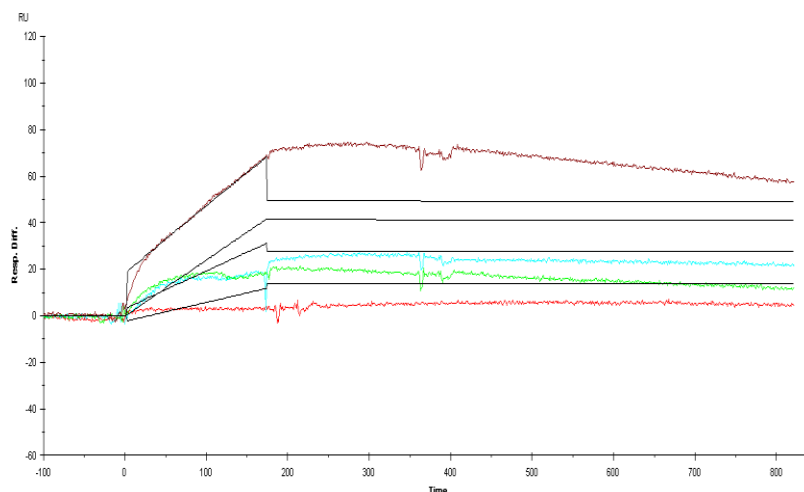


Figure 12. Evaluation of BM042 binding kinetics. The BM042 series (Figure 11) was plotted using BiaEval to obtain K_A and K_D kinetic binding constants in HBS-EP- K^+ buffer. The 5 μ M concentration was removed to provide better fitting data.

Table 3. Binding parameters of compound BM042. A series of kinetic binding parameters was obtained through the use of BiaEval to determine the affinity of the compound for the G-quadruplex substrate.

k_a (1/Ms)	k_d (1/s)	K_A (1/M)	K_D (M)	Chi^2
305	1.66e-5	1.84e7	5.45e-8	163

It should be noted that the fitting algorithm used does not accurately reproduce the dissociation curve but it does reflect the overall shape. The Chi^2 value is high, indicating the imprecise fit. In addition, the overall binding profile is very different from that of TMPyP4, which demonstrated rapid association and dissociation from the quadruplex structure (Figure 10, association region). When assayed in the presence of a similar quadruplex region, TMPyP4 displayed a dramatically higher rate of association, $k_a = 1.24e6$ (1/Ms) and rate of dissociation, $k_d = 0.155$ (1/s). Although the affinity for the

substrate was slightly lower, $K_A = 6.04e6$ (1/M), the strength of the bond that was formed remained relatively strong with $K_D = 1.71e-5$ (M) (55).

The next compound assayed was compound BM043 in a concentration series of 500 nM – 1.5 μ M (Figure 13). The concentrations of the compound in this series were lowered from the previous due to the strength observed in binding and the difficulty in removing the compound from the sensorchip during regeneration. This compound exhibited a much higher association rate than the previous as can be observed by the sharp increase in RU upon compound injection.

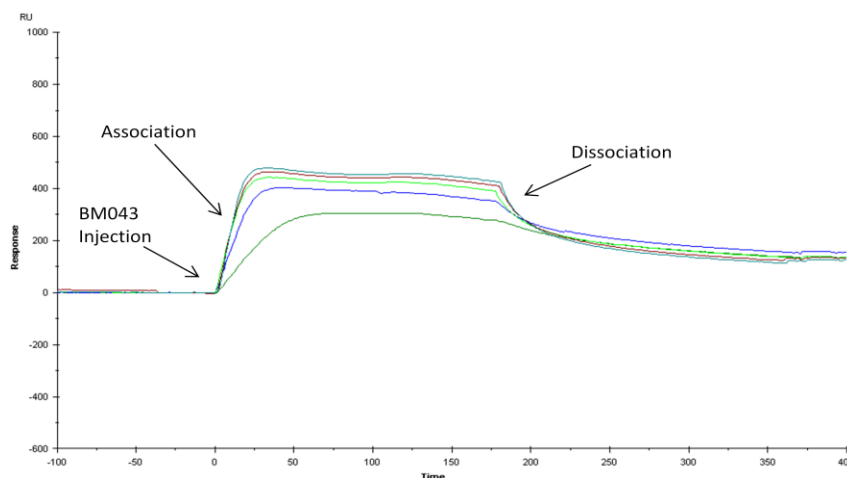


Figure 13. Compound BM043 concentration series. The compound BM043 was injected at 20 μ L/min in HBS-EP- K^+ buffer with varying concentrations consisting of 1.5 μ M (cyan trace), 1.2 μ M (maroon trace), 1 μ M (light green trace), 900 nM (dark blue trace), and 500 nM (forest trace). Each reference subtracted sensorgram represents binding of BM043 at the indicated concentration to ~150 RU of unhybridized imG4 DNA.

This compound was then plotted using BiaEval to determine binding parameters for comparison among compounds (Figure 14). This fitted evaluation showed a much higher association rate than BM042, $k_a = 6.35e5$ (1/Ms), and may be attributed to the

additional cationic charge on the molecule. With four cationic charges, this molecule appeared to bind very quickly to the negatively charged G-quadruplex. The dissociation of the compound was higher than expected, $k_d = 0.058$ (1/s), with much of the compound releasing rapidly upon completion of the injection, however, this rate slowed drastically with some interaction with the quadruplex persisting ($K_D = 9.17\text{e-}8$ [M]). The overall affinity for the G-quadruplex appeared comparable to the previous compound assayed at $K_A = 1.09\text{e}7$ (1/M).

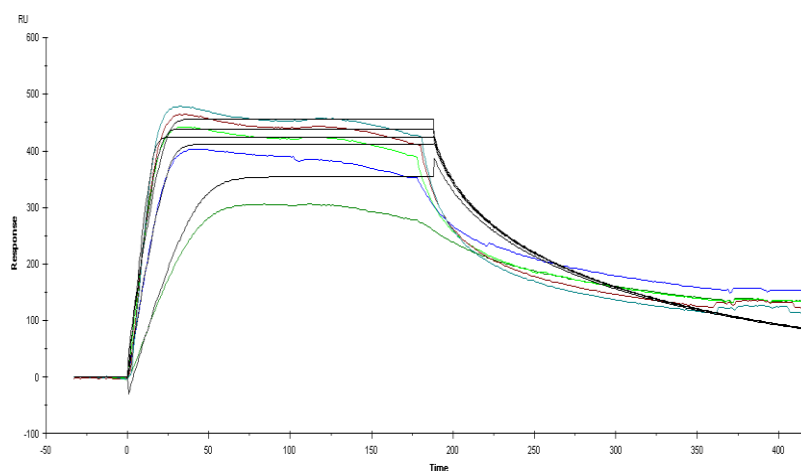


Figure 14. Evaluation of BM043 binding kinetics. The BM043 series (Figure 13) was plotted using BiaEval to obtain K_A and K_D kinetic binding constants in HBS-EP- K^+ buffer.

Table 4. Binding parameters of compound BM043. A series of kinetic binding parameters was obtained through the use of BiaEval to determine the affinity of the compound for the G-quadruplex substrate.

k_a (1/Ms)	k_d (1/s)	K_A (1/M)	K_D (M)	χ^2
6.35e5	0.058	1.09e7	9.17e-8	373

The next compound to be assayed was compound BM044 in a concentration series of 750 nM – 2 μ M. The concentrations in this series seemed to produce an efficient response in binding relative to the concentration used and displayed a similar response to compound BM042 with a slow association to the G-quadruplex (Figure 15). The greater association with the increased concentration may again exhibit cooperative binding effects or aggregation and this compound shares the same number of cationic charges as compound BM042, only differing by the substituent on the 4th porphyrin ‘arm’.

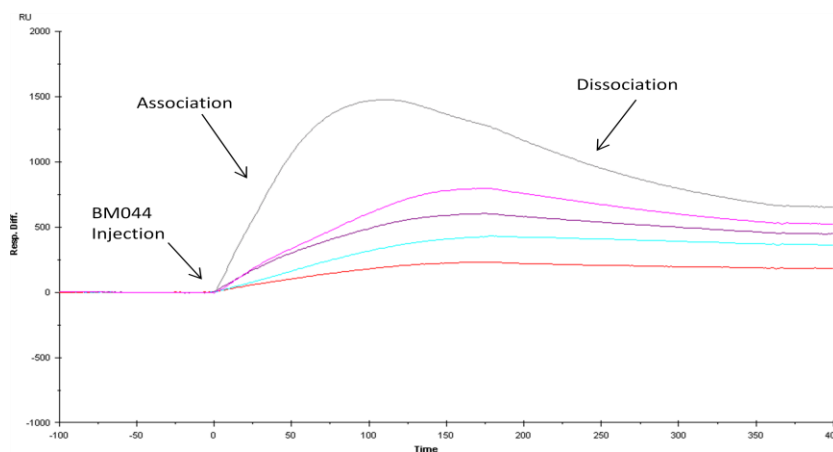


Figure 15. Compound BM044 concentration series. The compound BM044 was injected at 20 μ L/min in HBS-EP- K^+ buffer with varying concentrations consisting of 2 μ M (grey trace), 1.7 μ M (magenta trace), 1.2 μ M (dark purple trace), 900 nM (cyan trace), and 750 nM (red trace). Each reference subtracted sensorgram represents binding of BM044 to ~150 RU of unhybridized imG4 DNA to observe binding kinetics.

Compound BM044 was then plotted in BiaEval to obtain binding parameters for comparison among compounds (Figure 16). This evaluation revealed the lowest association rate of all compounds assayed, $k_a = 274$ (1/Ms). However, the compound dissociated more quickly from the G-quadruplex upon completion of the injection, $k_d = 2.42e-3$ (1/s), leading to the highest dissociation constant of all compounds assayed, $K_D = 8.8e-6$ (M). The lack of additional cationic charge seemed to give this compound a lower

affinity for the G-quadruplex with $K_A = 1.14e-5$ (1/M). Regeneration of this compound proved difficult due even though the K_D was fairly high, however, from observation of the concentration series (Figure 15) it appeared that the compound forms a strong, persistent interaction upon association with the substrate. Due to the fitting algorithm within the evaluation software, only 1:1 Langmuir binding interactions were obtainable and the poor kinetic fit for the compound may be due to multiple binding modes since the substrate contained single stranded and quadruplex forming regions (Table 5). Additional trials of the compound will be performed in future investigations, however, due to sensorchip degradation these could not be completed at this time.

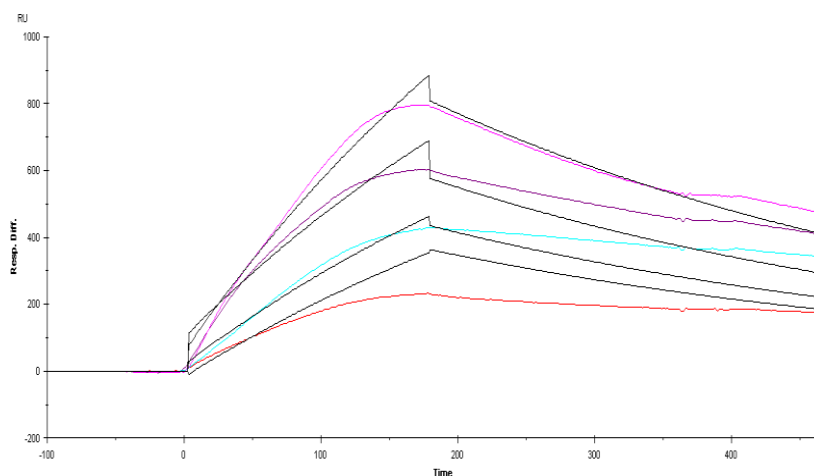


Figure 16. Evaluation of BM044 binding kinetics. The BM044 series (Figure 15) was plotted using BiaEval to obtain K_A and K_D kinetic binding constants in HBS-EP- K^+ buffer.

Table 5. Binding parameters of compound BM044. A series of kinetic binding parameters was obtained through the use of BiaEval to determine the affinity of the compound for the G-quadruplex substrate. The relatively high Chi^2 value obtained indicates a poor fit among the curves from the concentration series.

k_a (1/Ms)	k_d (1/s)	K_A (1/M)	K_D (M)	Chi^2
274	2.42e-3	1.14e5	8.8e-6	2.09e3

A 1 μM comparison of all compounds assayed thus far was performed to observe the binding of each compound compared to one another at a given concentration (Figure 17). These compounds appeared to follow the same trend in binding as previously shown, with BM042 associating slowest with the substrate, but also exhibiting the slowest rate of dissociation. It is interesting to note that TMPyP4 seemed to dissociate quickly from the substrate and will be beneficial in comparison of these compounds for inhibition trials.

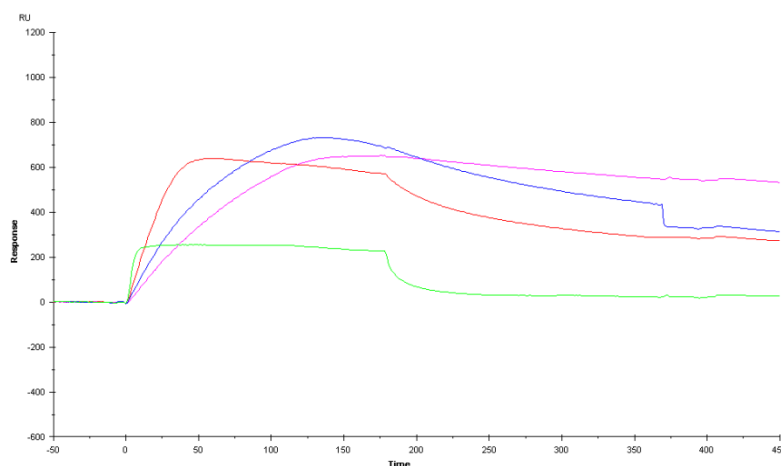


Figure 17. Comparison of compounds (1 μM). A solution (1 μM) of compound BM042 (magenta trace), BM043 (red trace), BM044 (blue trace), and TMPyP4 (light green trace) was injected at 20 $\mu\text{L}/\text{min}$ in HBS-EP- K^+ buffer. Each sensorgram was reference subtracted and represents binding of the indicated compound to ~ 150 RU of unhybridized imG4 DNA.

The compound 360 is a known selective G-quadruplex interactive agent (47). This compound was also assayed as a concentration series to determine binding kinetics for observation of affinity for the intramolecular imG4 substrate (Figure 18). This compound is different than the previous porphyrin analogues and is a crescent shaped molecule similar to Distamycin A, a compound with intercalation and groove binding capabilities in the presence of G-quadruplex structures. Concentrations of 500 nM – 5 μ M were investigated and appeared to have a very fast association rate as evident from the sensorgram. At concentrations greater than 1 μ M some aggregation may occur but dissociation was fairly rapid after the end of the injection.

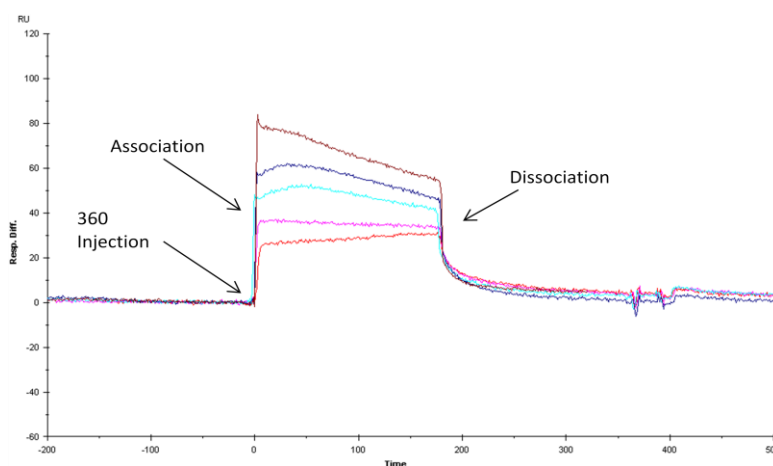


Figure 18. Compound 360 concentration series. The compound 360 was injected at 20 μ L/min in HBS-EP- K^+ buffer with varying concentrations consisting of 5 μ M (maroon trace), 3 μ M (blue trace), 2 μ M (cyan trace), 1 μ M (magenta trace), and 500 nM (red trace). Each reference subtracted sensorgram represents binding of 360 at the indicated concentration to \sim 375 RU of unhybridized imG4 DNA to observe binding kinetics.

Compound 360 was then subjected to evaluation using BiaEval for determination of binding parameters (Figure 19). This evaluation revealed the highest association of all compounds assayed, $k_a = 1.94e7$ (1/Ms), as was evident by the quick association

observed in the concentration series. When combined with the dissociation of the compound from the substrate, $k_d = 7.7e-3$, it was revealed that affinity for the G-quadruplex substrate was also the highest of all compounds assayed, $K_A = 2.52e9$ (1/M). The evaluation also revealed the tightest binding of all compounds with a $K_D = 3.96e-10$ (M), implying that 360 is capable of selectively binding G-quadruplex structures and maintaining a tight interaction at low concentrations. It is important to note that this compound produced the best fit among all compounds with a Chi^2 value of 7.91.

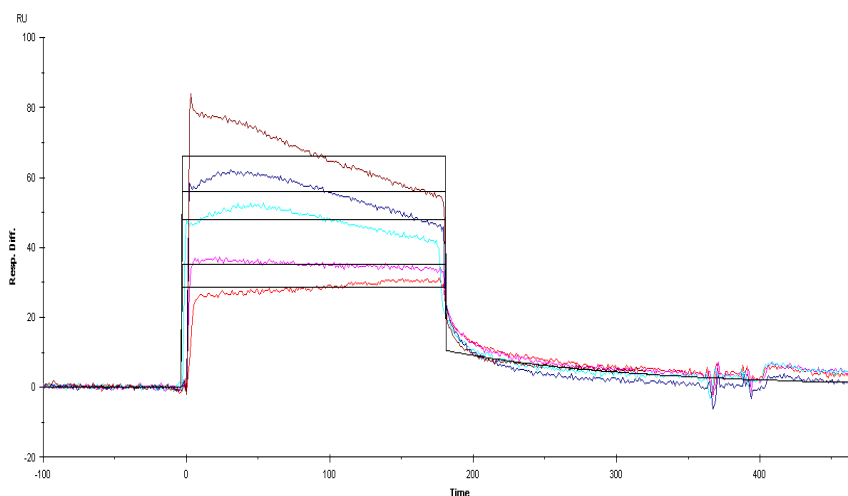


Figure 19. Evaluation of 360 binding kinetics. The 360 series (Figure 18) was plotted using BiaEval to obtain K_A and K_D kinetic binding constants in HBS-EP- K^+ buffer.

Table 6. Binding parameters of compound 360. A series of kinetic binding parameters was obtained through the use of BiaEval to determine the affinity of the compound for the G-quadruplex substrate.

k_a (1/Ms)	k_d (1/s)	K_A (1/M)	K_D (M)	Chi^2
1.94e7	7.7e-3	2.52e9	3.96e-10	7.91

These previous assays were all completed in the presence of HBS-EP-K⁺ to ensure proper quadruplex formation. The potassium ion for tetrad stability gives the best coordination with the eight oxygens present between the two tetrads and also provides a lower dehydration energy than other ions such as sodium or magnesium (56). Lithium has been shown to allow quadruplex formation, however, the extent to which the quadruplex forms is drastically lower than any other ion used for stabilization. Assays to determine the selectivity of compound binding to a destabilized G-quadruplex structure were accomplished through the use of a HBS-EP-LiCl₂ buffer. This buffer forced the immobilized intramolecular quadruplex to use lithium for quadruplex formation which should result in a drastically decreased amount of quadruplex available for binding. Circular dichroism was performed to assess the effects of HBS-EP-LiCl₂ buffer compared to a HBS-EP-K⁺ buffer on the structure of a similar DNA oligonucleotide containing the same G-quadruplex folding motif (Figure 20). This evaluation showed a marked chromophoric shift that correlates with published literature for a change in the G-quadruplex structure and intensity (57).

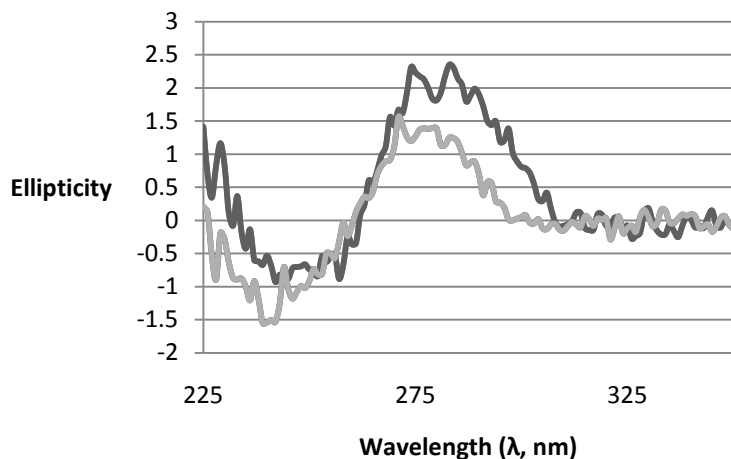


Figure 20. CD spectroscopy for evaluating buffer effects on DNA topology. Circular dichroism spectroscopy investigation of nucleic acid quadruplex formation was performed in the presence of HBS-EP- K^+ buffer (dark gray) and HBS-EP- $LiCl_2$ buffer.

Compound BM042 was then assayed in HBS-EP- $LiCl_2$ for determination of binding parameters to assess the influence and selectivity for a destabilized G-quadruplex structure (Figure 21). This concentration series (200nM – 800 nM) displayed a much lower response than previously observed in HBS-EP- K^+ buffer.

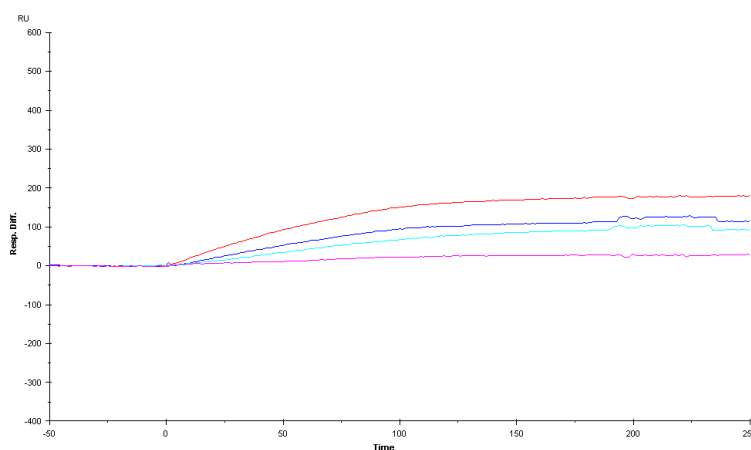


Figure 21. Compound BM042 lithium concentration series. The compound BM042 was injected at 20 μ L/min in HBS-EP- $LiCl_2$ buffer with varying concentrations consisting of 800 nM (red trace), 600 nM (blue trace), 400 nM (light blue trace), and 200 nM (magenta trace). Each sensorgram represents binding of BM042 at the indicated concentration to \sim 150 RU of unhybridized imG4 DNA to observe binding kinetics.

While additional concentrations of the compounds would be beneficial for analysis, the evaluation of BM042 (Figure 22) showed that there is a dramatic decrease in the association of compound with the destabilized quadruplex substrate, $k_a = 38.1$ (1/Ms). In coordination with an increase of dissociation of the compound from the substrate, $k_d = 7.06 \times 10^{-3}$ (1/s), the overall affinity of the compound was reduced dramatically, $K_A = 5.39 \times 10^3$ (1/M). The dissociation constant was also the highest of all assays, $K_D = 1.86 \times 10^{-4}$, indicating a much higher concentration of compound was required for binding. From this determination, it was concluded that BM042 was selective for quadruplex over single-stranded DNA.

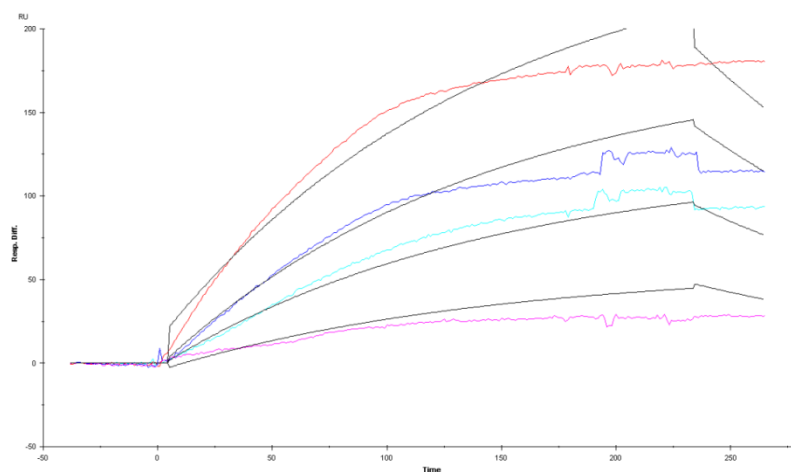


Figure 22. Evaluation of BM042 binding kinetics. The lithium BM042 series (Figure 21) was plotted using BiaEval to obtain K_A and K_D kinetic binding constants in HBS-EP- LiCl_2 buffer.

Table 7. Binding parameters of compound BM042 in lithium. A series of kinetic binding parameters was obtained through the use of BiaEval to determine the affinity of the compound for the G-quadruplex substrate.

k_a (1/Ms)	k_d (1/s)	K_A (1/M)	K_D (M)	Chi ²
38.1	7.06e-3	5.39e3	1.86e-4	56.6

All porphyrin analogue compounds were then diluted to a 500 nM concentration in HBS-EP-LiCl₂ buffer and assayed for direct comparison of their ability to bind destabilized G-quadruplex structures (Figure 23). This assessment showed a decrease in the overall response when compared to HBS-EP-K⁺ buffer indicating a lowered association of each compound for the destabilized structure. Each compound appeared to slowly associate and remain bound to the substrate. The low amount of persistent binding was likely electrostatic, non-specific binding, indicating a relatively low affinity for the unstable lithium ion G-quadruplex versus the potassium ion-stabilized structure.

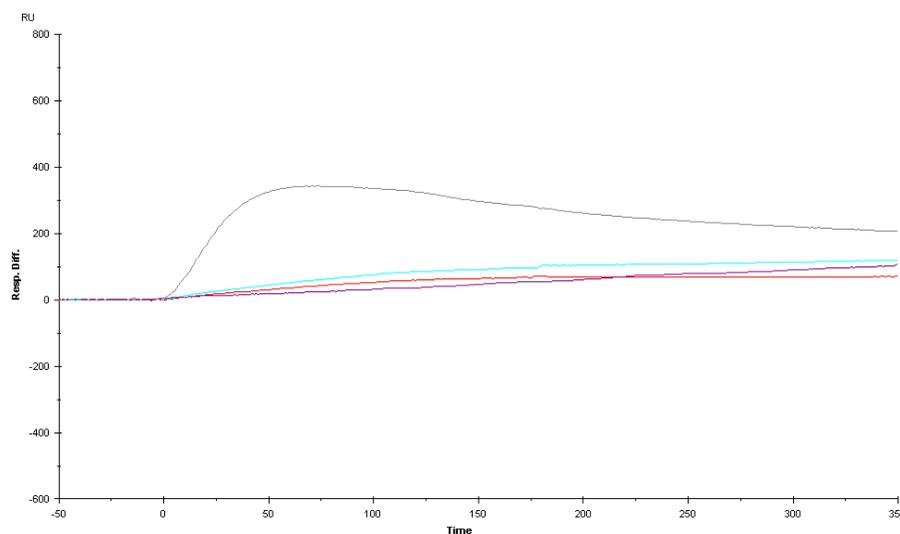


Figure 23. Lithium binding comparison of compounds. A 500 nM concentration of compounds BM042 (red trace), BM043 (light blue trace), BM044 (magenta trace), and TMPyP4 (gray trace) were injected in HBS-EP-LiCl₂ buffer at 20 μ L/min. Each sensorgram was reference subtracted and represents binding of the indicated compound to ~150 RU of unhybridized imG4 DNA.

The SA chip was then evaluated to assess the condition of the chip after finishing the lithium studies (Figure 24). HBS-EP-K⁺ buffer was used to inject 500 nM concentrations of compounds BM042 and TMPyP4 in the presence of the stabilized intramolecular quadruplex structure. This assay showed a response similar to the ones observed previously for both compounds indicating that chip degradation had not taken place and that HBS-EP-LiCl₂ was causing the effect of lowered response compared to previous trials.

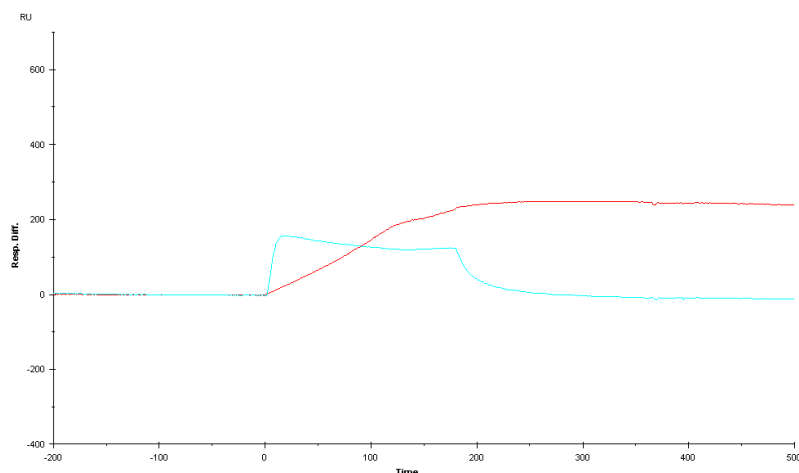


Figure 24. Evaluating SA chip condition. A 500 nM injection of compounds BM042 (red trace) and TMPyP4 (light blue trace) were injected in HBS-EP-K⁺ buffer to investigate the current SA chip conditions with those of previously elucidated binding curves. Each sensorgram was reference subtracted and represents binding of the indicated compound to ~150 RU of unhybridized imG4 DNA.

3b. Inhibition of LTag helicase activity with G-quadruplex interactive compounds

Prior to investigating LTag inhibition with the porphyrin analogs and 360, LTag enzymatic activity was normalized again due to the necessity of purchasing new LTag (Figure 25). This assay used varying enzyme concentration to deduce a sub-optimal enzymatic activity in the presence of an intramolecular G-quadruplex structure. Using a 15 mM ATP concentration, the LTag concentration was lowered to 1.0 nM to effectively bring the enzymatic activity to ~70%. Each assay was performed in HBS-EP-K⁺ buffer with 430 RU of immobilized imG4 DNA. The immobilized substrate was then fully hybridized with partially complementary imG4comp2 DNA (127 RU). Using equation (2), enzymatic activity was calculated based upon the removal of the DNA complement by LTag.

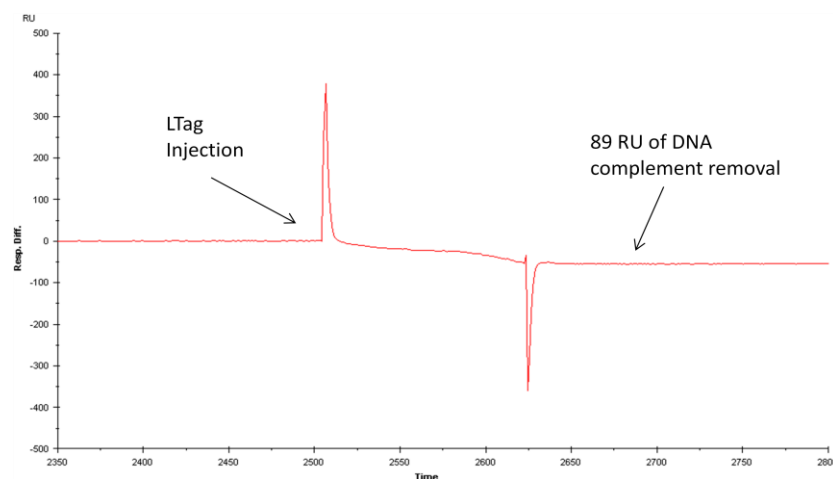


Figure 25. Determining decreased enzymatic activity. This assay used varying concentrations of LTag to determine a stable reduced enzyme activity in the presence of G-quadruplex structures. This figure contains ~127 RU of hybridized imG4comp2 DNA and following LTag injection, 89 RU are removed providing a 70% activity. Each trial is reference subtracted and performed on an SA chip in HBS-EP-Mg²⁺ buffer.

Upon reaching a stable, reduced enzymatic activity, inhibition trials using G-quadruplex interactive compounds were performed. Each trial used a fully hybridized DNA substrate in HBS-EP-Mg²⁺ buffer for proper LTag activity. The enzymatic activity produced from each trial was calculated by the amount of substrate loss divided by the full RU loss seen of the reduced activity enzyme, equation (3). The first compound to be assayed was compound BM042, which showed a comparable binding event to previous studies followed by a decrease in overall RU once LTag was introduced (Figure 26). The enzyme activity after two runs with compound BM042 was calculated to be 47%, a reduced activity of the enzyme from the interaction of BM042 with the DNA substrate.

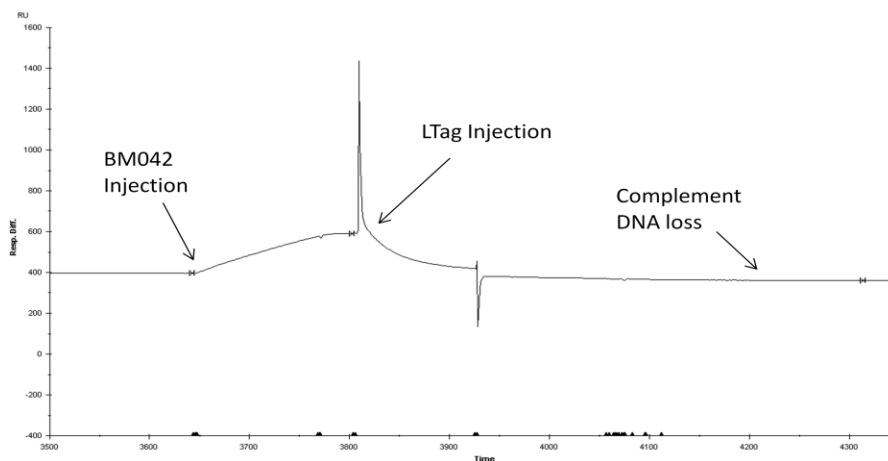


Figure 26. BM042 inhibition of LTag. A 1 μM concentration of compound BM042 was injected at 20 $\mu\text{L}/\text{min}$ in HBS-EP- Mg^{2+} buffer in manual inject mode for 120 seconds, immediately followed by 1 nM LTag/15 mM ATP injection and allowed to stabilize to determine inhibitory effects. Each trial was reference subtracted.

Compound BM043 was then assayed for LTag enzyme inhibition using the same conditions as previously stated. This compound also showed a proportional binding response as previously elucidated indicating that addition of magnesium to buffer conditions did not alter compound binding to the substrate. Again, upon addition of BM043 to the substrate, reduced activity LTag was injected to determine potential enzymatic inhibition (Figure 27). The enzymatic activity calculated from BM043 showed that full inhibition occurred, as no DNA loss was evident and compound remained firmly bound to the substrate. While this compound did not display the highest affinity for the quadruplex or tightest formation to the substrate, it fully inhibited the enzymatic activity of LTag.

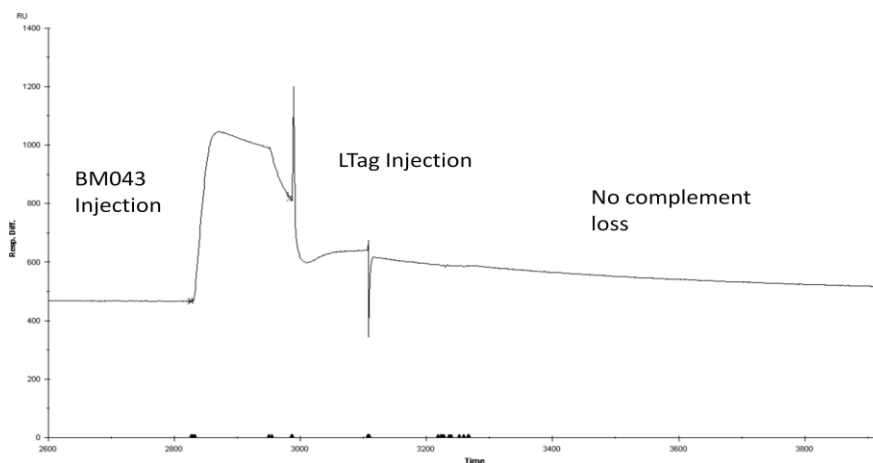


Figure 27. BM043 inhibition of LTag. A 1 μM concentration of compound BM043 was injected at 20 $\mu\text{L}/\text{min}$ in HBS-EP- Mg^{2+} buffer in manual inject mode for 120 seconds, immediately followed by 1 nM LTag/15 mM ATP injection and allowed to stabilize to determine inhibitory effects. Each trial was reference subtracted.

Next, compound BM044 was assayed to determine inhibitory effects of LTag. Showing comparable binding to previous assessments, this compound also provided complete inhibition, reducing enzyme activity to 0% (Figure 28).

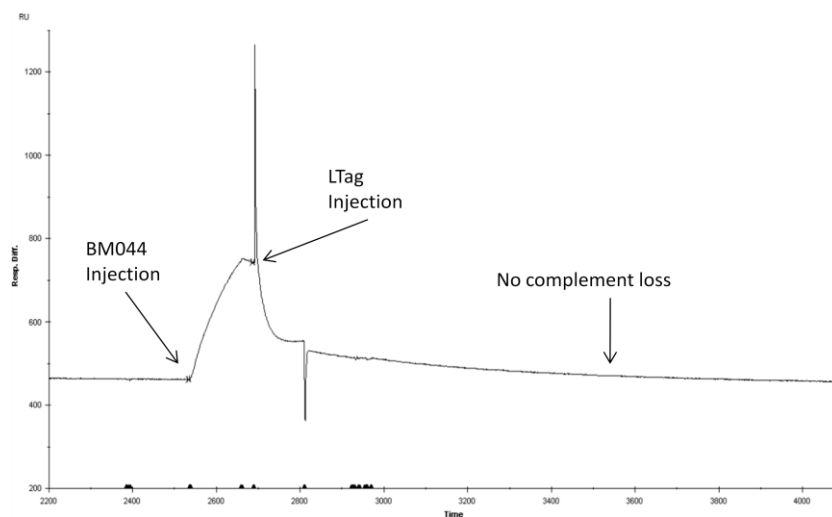


Figure 28. BM044 inhibition of LTag. A 1 μM concentration of compound BM044 was injected at 20 $\mu\text{L}/\text{min}$ in HBS-EP- Mg^{2+} buffer in manual inject mode for 120 seconds, immediately followed by 1 nM LTag/15 mM ATP injection and allowed to stabilize to determine inhibitory effects. Each trial was reference subtracted.

Finally, compound 360 was assayed under the same conditions as previously stated to determine inhibition of enzymatic activity. Upon interaction with the DNA substrate, LTag was injected and complement DNA loss was observed (Figure 29). Showing a 16.8% enzyme activity, 360 appeared to be an ideal inhibitor of LTag activity when combined with its selectivity for G-quadruplex structures and its tight binding once association occurred.

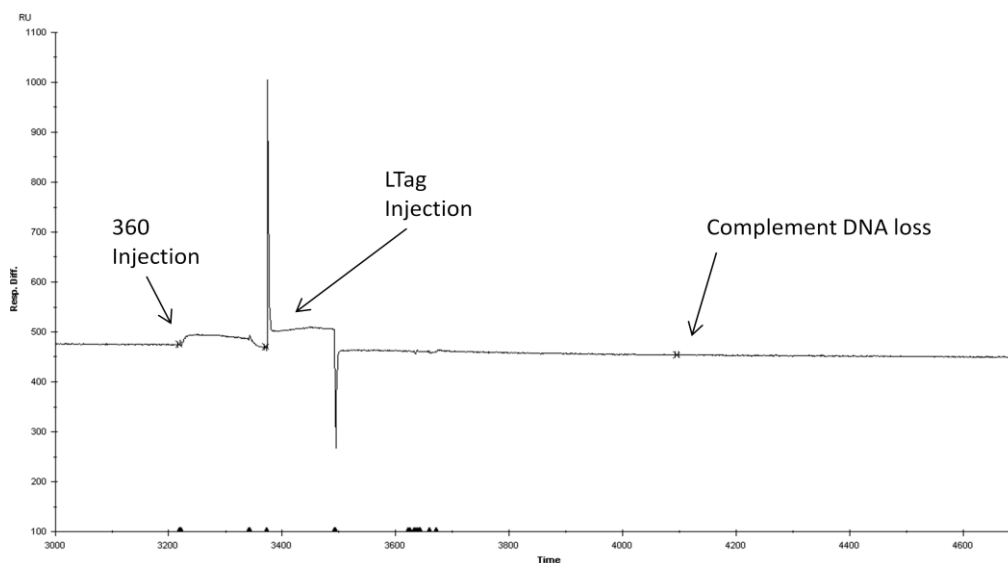


Figure 29. 360 inhibition of LTag. A 1 μ M concentration of compound 360 was injected at 20 μ L/min in HBS-EP-Mg² buffer in manual inject mode for 120 seconds, immediately followed by 1 nM LTag/15 mM ATP injection and allowed to stabilize to determine inhibitory effects. Each trial was reference subtracted.

4. Summary

Assays to investigate the binding parameters of novel compounds were performed using SPR based analysis. Many of these compounds exhibited similar structures with minor variations, however, they each produced varying results in aspects of association, dissociation, affinity for the G-quadruplex, and how tightly each compound is capable of

binding the DNA substrate. Further investigation into this structure/function relationship through additional compounds would be beneficial as well as continued assessment of current compounds that show potentially promising results. Compound 360 showed high selectivity for the G-quadruplex structure and produced decreased levels of LTag activity during inhibition assays, making it a viable candidate for continued research. The crescent shape of this molecule may interact in a more appropriate manner than the terminal stacking features of the larger porphyrine derivatives and continued synthesis of similar compounds with varying charge may provide additional insight to potential chemotherapeutic agents. Continued assessment of these novel compounds, as well as future compounds, will surely lead to scientific advancement in the field of biochemistry.

Table 8. Summary of binding and inhibition data. This table summarizes the binding affinity and reduction of enzyme activity for each compound assayed. Compound 360 shows potential for continued research due to high affinity in conjunction with enzymatic activity reduction of LTag.

Compound	K_A (1/M)	% Unwinding
BM042	1.84e7	47%
BM043	1.09e7	0%
BM044	1.14e5	0%
360	2.52e9	17%

REFERENCES

1. Bullock, P.A. (1997) The initiation of simian virus 40 DNA replication in vitro. *Crit. Rev. Biochem. Mol. Biol.* **32**, 503–568.
2. Simmons, D.T. (2000) SV40 large T antigen: functions in DNA replication and transformation. *Adv. Virus Res.* **55**, 75–134.
3. Martini, F., Corallini A., Balatti, V., Sabbioni, S., Pancaldi, C., and Tognon, M. (2007) Simian virus 40 in humans. *Infectious Agents and Cancer.* **2**, 13.
4. Alwine, J.C. (1982) Evidence for simian virus 40 late transcriptional control: mixed infections of wild-type simian virus 40 and a late leader deletion mutant exhibit trans effects on late viral RNA synthesis. *J. Virol.* **42**, 798-803.
5. Hay, N., Skolnick-David, H., and Aloni, Y. (1982) Attenuation in the control of SV40 gene expression. *Cell.* **29**, 183-193.
6. Norkin, L.C. (1999) Simian virus 40 infection via MHC class I molecules and caveolae. *Immunol. Rev.* **168**, 13-22.
7. Dornreiter, I., Hoss, A., Arthur, A.K., and Fanning, E. (1990) SV40 T antigen binds directly to the large subunit of purified DNA polymerase alpha. *EMBO J.* **9**, 3329-3336.
8. Melendy, T. and Stillman, B. (1993) An interaction between replication protein A and SV40 T antigen appears essential for primosome assembly during SV40 DNA replication. *J. Biol. Chem.* **268**, 3389-3395.
9. Flint, S.J., Racaniello, V.R., Enquist, L.W., Skalka, A.M., and Krug, R.M. (2000) *Principles of Virology: Molecular Biology, Pathogenesis, and Control*, ASM Press, Washington, D.C.
10. Stahl, H., Droge, P., and Knippers, R. (1986) DNA helicase activity of SV40 large tumor antigen. *EMBO J.*, **5**, 1939-1944.
11. DeLucia, A.L., Deb, S., Partin, K., and Tegtmeyer, P. (1986) Functional interactions of the simian virus 40 core origin of replication with flanking regulatory sequences. *J. Virol.*, **57**, 138–144.

12. Dean, F.B., Borowiec J.A., Ishimi Y., Deb S., Tegtmeyer P., and Hurwitz J. (1987) Simian virus 40 large tumor antigen requires three core replication origin domains for DNA unwinding and replication in vitro. *Proc. Natl. Acad. Sci.* **84**, 8267–8271.
13. Deb, S., Delucia, A.L., Koff, A., Tsui, S., and Tegtmeyer, P. (1986) The adenine-thymine domain of the simian virus 40 core origin directs DNA bending and coordinately regulates DNA replication. *Mol. Cell. Biol.*, **6**, 4578-4584.
14. Bochkareva, E., Martynowski D., Seitova A., and Bochkarev A. (2006) Structure of the origin-binding domain of simian virus 40 large T antigen bound to DNA. *EMBO J.* **25**, 5961–5969.
15. Koonin, E.V., Aravind, L., and Iyer, L.M. (2001) Common origin of four diverse families of large eukaryotic DNA viruses. *J. Virol.* **75**, 23.
16. Berjanskii, M.V., Riley, M.I., Xie, A., Semenchenko, V., Folk, W.R., and Van Doren, S.R. (2000) NMR structure of the N-terminal J domain of murine polyomavirus T antigens: implications for DnaJ-like domains and for mutations of T antigens. *J. Biol. Chem.* **275**, 36094–36103.
17. Lee, J.O., Russo, A.A., and Pavletich, N.P. (1998) Structure of the retinoblastoma tumour-suppressor pocket domain bound to a peptide from HPV E7. *Nature.* **391**, 859–865.
18. Sullivan, C.S. and Pipas, J.M. (2002) T Antigens of Simian Virus 40: Molecular Chaperones for Viral Replication and Tumorigenesis. *Micro. Biol. & Mol. Biol. Rev.* **66**, 179-202.
19. Weisshart, K., Taneja, P., Jenne, A., Herbig, U., and Simmons, D.T. (1999) Two regions of simian virus 40 T antigen determine cooperativity of double hexamer assembly on the viral origin of DNA replication and promote hexamer interactions during bidirectional origin DNA unwinding. *J. Virol.* **73**, 2201–2211.
20. Smelkova, N.V. and Borowiec, J.A. (1997) Dimerization of simian virus 40 T antigen hexamers activates T antigen DNA helicase activity. *J. Virol.* **71**, 8766–8773.
21. Gai, D., Zhao, R., Li, D., Finkielstein, C.V., and Chen, X.S. (2004) Mechanisms of conformational change for a replicative hexameric helicase of SV40 large tumor antigen. *Cell.* **119**, 47-60.
22. Reese, D.K., Sreekumar, K.R., and Bullock, P.A. (2004) Interactions required for binding of simian virus 40 T antigen to the viral origin and molecular modeling of initial assembly events. *J. Virol.* **78**, 2921–2934.

23. Khopde, S. and Simmons, T. (2007) Simian virus 40 DNA replication is dependent on an interaction between topoisomerase I and the C-terminal end of T antigen. *J. Virol.* **82**, 1136-1145.
24. Sengupta, D.J. and Borowiec, J.A. (1992) Strand-Specific Recognition of a Synthetic DNA Replication Fork by the SV40 Large Tumor Antigen. *Science.* **256**, 1656-1661.
25. Baran, N., Pucshansky, L., Marco, Y., Benjamin, S., and Manor, H. (1997) The SV40 large T antigen helicase can unwind four stranded DNA structures linked by G-quartets. *Nucl. Acids Res.* **25**, 297-303.
26. Williamson, J.R. (1994) G-quartet structures in telomeric DNA. *Annu Rev. Biophys. Biomol. Struct.* **23**, 703-730.
27. Gilber, D.E. and Feigon, J. (1999) Multistranded DNA structures. *Curr. Opin. Struct. Biomol.* **9**, 305-314.
28. Burge, S., Parkinson, G.N., Hazel, P., Todd, A.K., and Neidle, S. (2006) Quadruplex DNA: sequence, topology, and structure. *Nucl. Acids Res.* **34**, 5402-5415.
29. Sen, D. and Gilbert, W. (1992) Guanine quartet structures. *Methods Enzymol.* **211**, 191-199.
30. Huppert, J.L. and Balasubramanian, S. (2005) Prevalence of quadruplexes in the human genome. *Nucl. Acids Res.* **33**, 2906-2916.
31. Crabbe, L., Verdun, R.E., Haggblom, C.I., and Karlseder, J. (2004) Defective telomere lagging strand synthesis in cells lacking WRN helicase activity. *Science.* **306**, 1951-1953.
32. Wang, Y. and Patel, D.J. (1993) Solution structure of the human telomeric repeat d[AG3(T2AG3)3] G-tetraplex. *Structure*, **1**, 263-282.
33. Parkinson, G.H., Lee, M.P.H., and Neidle, S. (2002) Crystal structure of parallel quadruplexes from human telomeric DNA. *Nature*, **417**, 876-880.
34. Schulz V.P., Zakian V.A., Ogburn C.E., McKay J., Jarzebowicz A.A., Edland S.D., and Martin G.M. (1996) Accelerated loss of telomeric repeats may not explain accelerated replicative decline of Werner syndrome cells. *Hum. Genet.* **97**, 750-754.
35. Gearhart J., Pashos E.E., and Prasad M.K., Pluripotency Redux -- advances in stem-cell research, *N. Engl. J. Med.* **357**, 1469.

36. Bergsagel, P.L. and Kuehl, W.M. (2001) Chromosome translocations in multiple myeloma. *Oncogene*. **20**, 5611-5622.
37. Duquette M.L., Pham P., Goodman M.F., and Maizels N. (2005) AID binds to transcription-induced structures in c-MYC that map to regions associated with translocation and hypermutation. *Oncogene*. **24**, 5791-5798.
38. Kim, N.W., Piatyszek, M.A., and Prowse, K.R. (1994) Specific association of human telomerase activity with immortal cells and cancer. *Science*. **266**, 2011–2015.
39. Pagano, B. and Giancola, C. (2007) Energetics of quadruplex-drug recognition in anticancer therapy. *Curr. Cancer Drug Targets*. **7**, 520–540.
40. Zahler, A.M., Williamson, J.R., Cech, T.R., and Prescott, D.M. (1991) Inhibition of telomerase by G-quartet DNA structures. *Nature*. **350**, 718-720.
41. Kim, N.W., Piatysek, M.A., Prowse, K.R., Harley, C.B., West, M.D., Ho, P.L.C., Coviello, G.M., Wright, W.E., Weinrich, S.L., and Shay, J.W. (1994) Specific association of human telomerase activity with immortal cells and cancer. *Science*. **266**, 2011-2015.
42. Phan, A.T. and Patel, D.J. (2003) Two-repeat human telomeric d(TAGGGTTAGGGT) sequence forms interconverting parallel and antiparallel G-quadruplexes in solution: distinct topologies, thermodynamic properties, and folding/unfolding kinetics. *J. Am. Chem. Soc.* **125**, 15021-15027.
43. Sehlstedt, U., Kim, S.K., Carter, P., Goodisman, J., Vollano, J.F., Norden, B., and Dabrowiak, J.C. (1994) Interaction of cationic porphyrins with DNA. *Biochemistry*. **33**, 417-426.
44. Pagano, B., Fotticchia, I., De Tito, S., Mattia, C.A., Mayol, L., Novellino, E., Randazzo, A., and Giancola, C. (2010) Selective binding of distamycin A derivative to G-quadruplex structure [d(TGGGGT)]₄. *J. Nucl. Acids*. **2010**, 247137.
45. Sharma, S., Doherty, K.M., and Brosh, R.M. (2005) DNA helicases as targets for anti-cancer drugs. *Curr. Med. Chem. Anticancer Agents*. **5**, 183-199.
46. Plyler, J. (2009) Monitoring SV40 large T antigen helicase activity using surface Plasmon resonance. Texas State University-San Marcos.

47. Pennarun, G., Granotier, C., Gauthier, L.R., Gomez, D., Hoffschir, F., Mandine, E., Riou, J.F., Mergny, J.L., Mailliet, P., and Boussin, F.D. (2005) Apoptosis related to telomere instability and cell cycle alterations in human glioma cells treated by new highly selective G-quadruplex ligands. *Oncogene*. **18**, 2917-2928.
48. Schuck, P. (1997) Use of surface plasmon resonance to probe the equilibrium and dynamic aspects of interactions between biological macromolecules. *Annu. Rev. Biophys. Biomol. Struct.* **26**, 541-566.
49. Garland, P.B. (1996) Optical evanescent wave methods for the study of biomolecular interactions. *Q. Rev. Biophys.* **29**, 91-117.
50. Karlsson, R., Roos, H., Fagerstam, L., and Person, B. (1994) Kinetic and concentration analysis using BIA technology. *Methods: Companion Methods Enzymol.* **6**, 99-110.
51. Yeung, D., Gill, A., Maule, C.H., and Davies, R.J. (1995) Detection and quantification of biomolecular interactions with optical biosensors. *J. Immunol. Methods*. **183**, 175-182.
52. Lofas, S. and Johnsson, B. (1990) A novel hydrogel matrix on gold surfaces in surface plasmon resonance sensors for fast and efficient covalent immobilization of ligands. *J. Chem. Soc. Chem. Commun.* **21**, 1526-1528.
53. Gitlin, G., Bayer, E.A., and Wilchek, M. (1987) Studies on the biotin-binding sites of avidin and streptavidin. Tyrosine residues are involved in the binding site. *J. Biochem.* **242**, 923-926.
54. Wheelhouse, R.T., Sun, D., Han, H., Han, F., and Hurley, L.H. (1998) Cationic porphyrins as telomerase inhibitors: the interaction of tetra-(*N*-methyl-4-pyridyl) porphine with quadruplex DNA. *J. Am. Chem. Soc.* **120**, 3261-3262.
55. Tuesuwan, B., Jonathan, K.T., Thomas, P.W., Rodriguez, M., Li, J., David, W.M., and Kerwin, S.M. (2008) Simian Virus 40 Large T-Antigen G-Quadruplex DNA Helicase Inhibition by G-Quadruplex DNA-Interactive Agents. *Biochemistry*. **47**, 1896 -1909.
56. Hud, N.V. and Plavec, J. (2006) The role of cations in determining quadruplex structure and stability. *Quadruplex Nucleic Acids*. Royal Society of Chemistry Publishing, Cambridge UK; pp. 100–130.
57. Balkwill, G.D., Garner, T.P., Williams, H.E.L., and Searle, M.S. (2009) Folding topology of a bimolecular DNA quadruplex containing a stable mini-hairpin motif within the diagonal loop. *J. Mol. Biol.* **385**, 1600-1615.

VITA

Matthew Decker was born in Baton Rouge, Louisiana on October 18th, 1985, the son of Douglas B. Decker and Julie M. Decker. He moved to Bastrop, Texas in 2000 to finish his high school education at Bastrop High School. Upon completion, he enrolled in Texas State University-San Marcos where he received his first degree in animal science and a minor in biochemistry. After graduation, he began post-baccalaureate work for the College of Science in the field of biochemistry. He worked at Tickle-Blagg Animal Hospital as a veterinary technician through the duration of his collegiate education, where after, he was accepted to Texas A&M University College of Veterinary Medicine and Biomedical Sciences to pursue his ultimate goal of becoming a veterinarian.

Permanent Address: 20201 Grand Banks Lane

Pflugerville, TX 78660

This thesis was typed by Matthew J. Decker